PERGAMON

International Journal of Plasticity 19 (2003) 1679–1713

INTERNATIONAL JOURNAL OF Plasticity

www.elsevier.com/locate/ijplas

An anisotropic ductile damage model based on irreversible thermodynamics

Michael Brünig*

Lehrstuhl für Baumechanik- Statik, Universität Dortmund, August-Schmidt-Str. 8, D-44221 Dortmund, Germany

Received in final revised form 24 September 2002

Abstract

The paper deals with fundamental constitutive issues in the elastic–plastic-damage rate theory and the numerical modelling of the large strain elastic–plastic deformation behavior of anisotropically damaged ductile metals. The proposed model is based on a generalized macroscopic theory within the framework of nonlinear continuum damage mechanics taking into account kinematic description of damage. It employs the consideration of damaged as well as fictitious undamaged configurations related via metric transformations which lead to the definition of damage strain tensors. The modular structure of the continuum theory is accomplished by the kinematic decomposition of strain rates into elastic, plastic and damage parts. To be able to address both the plastic flow and the anisotropic damage process, respective Helmholtz free energy functions of the fictitious undamaged configuration and of the current damaged configuration are introduced separately. A generalized yield condition based on invariants of the effective stress tensor is used to adequately describe the plastic flow properties of ductile metals and the plastic strain rate tensor is determined by a non-associated flow rule. Considering the damaged configurations a damage criterion is formulated using stress components referred to the elastically unloaded damage configuration. The damage strain rate tensor takes into account isotropic as well as anisotropic effects providing a realistic physical representation of ductile material degradation. Identification of material parameters is discussed in some detail. The applicability of the proposed continuum damage theory is demonstrated by numerical simulation of the inelastic deformation process of tension specimens.

Keywords: A. Microcracking; A. Voids and inclusions; B. Elastic–plastic material; B. Finite strain; C. Finite elements

* Tel.: +49-231-755-4682; fax: +49-231-755-2532.
E-mail address: michael.bruenig@uni-dortmund.de (M. Brünig).

0749-6419/03/$ - see front matter
PII: S0749-6419(02)00114-6

1. Introduction

The accurate and realistic description of inelastic behavior of ductile metals is essential for the solution of numerous boundary-value problems occurring in mechanical and civil engineering. For example, microscopic defects and cracks cause reduction in strength of materials and shorten the life time of engineering structures. Therefore, a main issue in engineering applications is to provide realistic information on the stress distribution within elements of such materials or assessment of safety factor against failure. During the past decades the constitutive modelling of ductile damaged materials in the finite deformation range has received considerable attention, as can be seen from a large number of bibliographies, reviews and discussions given, for example, by Chaboche (1988a,b), Krajcinovic (1989), Tvergaard (1990), Lemaitre (1996), and Voyiadjis and Kattan (1999).

Continuum damage mechanics discusses systematically the effects of damage on the mechanical properties of materials and structures as well as the influence of external conditions and damage itself on the subsequent development of damage. Critical values of damage variables might be viewed as a major parameter at the onset of failure. An important issue in such phenomenological constitutive models is the appropriate choice of the physical nature of mechanical variables describing the damage state of materials and their tensorial representation. To be able to describe the gradual internal deterioration of ductile metals within the framework of continuum thermodynamics several continuum damage models have been proposed which are either phenomenological or micromechanically based, see Brünig (2001) for an overview. Namely, scalar valued damage variables have been proposed by Kachanov (1958), Rabotnov (1963), Lemaitre (1985a,b), Lemaitre and Dufailly (1987) and Alves (2001) among many others, whereas Krajcinovic and Fonseka (1981a,b) and Krajcinovic (1983) employed an axial vector representation. In addition, to be able to take into account damage induced material anisotropy, second order damage tensors have been introduced e.g. by Kachanov (1980), Murakami and Ohno (1981), Betten (1982, 1983), Krajcinovic (1983), Chow and Wang (1987), Murakami (1988), Ju (1990), Lu and Chow (1990), Baste and Audoin (1991), Voyiadjis and Kattan (1992), Bruhns and Schiesse (1996), and Steinmann and Carol (1998), and fourth rank damage tensors were already introduced, for example, in the anisotropic creep damage modelling by Chaboche (1984). Furthermore, various order damage tensors and their relationship to some typical two- and three-dimensional crack density distributions were analyzed by Lubarda and Krajcinovic (1993). Efforts have been made to develop theories of ductile fracture based upon the nucleation and growth of voids during straining and upon plastic flow localization into narrow bands within the deforming porous regions which then become the sites of macrofracture development. An overview and classification of available models in local approach of fracture are given by Lemaitre (1986). Hence, accurate and efficient constitutive models of damaged ductile materials are needed as the basis for a theory of ductile fracture.

The applicability of an accurate material model requires specification of the significant macroscopic and microscopic features of the material structure. It has been

observed in metallurgical tests that nucleation of microvoids and their growth and coalescence are the main steps toward the formation of a mesocrack in ductile materials, which eventually leads to failure. This behavior affects various local and averaged material properties such as the elastic constitutive parameters (see e.g. Lemaitre and Dufailly, 1987). These property changes are indicative of material degradation, and their measurement can be used to determine appropriate damage variables in engineering materials. For example, Alves et al. (2000) and Alves (2001) reported of some damage measurements using different experimental techniques. Their results indicate different values for the damage parameters on the same specimen according to the definition of damage and to the experimental technique employed and, therefore, damage is an adjustable parameter. Thus, the choice of the most appropriate damage measure is not an easy task and the damage parameter determined experimentally must be carefully related to the theoretical model.

However, scatter of experimental data associated with machine precision, testing techniques, and statistical variation of material properties from one sample to another is a main factor enforcing the notion that the primary goal of the engineering applicability of any constitutive model should be set in the prediction of essential features of experimentally observed behavior, rather than in replicating the entire history of stress–strain curves. Along this line it should also be emphasized that numerical implementation of a proposed constitutive model into an accurate and efficient computer code is almost as important as the material model itself. Therefore, there is a need for constitutive models which would sufficiently accurately and numerically efficiently simulate the stress–strain behavior of engineering materials and describe progressive damage during deformation. Nowadays, it is well known that nucleation and growth of microcracks are governed by large strains of the material itself and lead to deterioration of macroscopic elastic properties. Two principal consequences are the diminution of the elastic stiffness as well as the induced material anisotropy.

In order to develop an elaborate theory for the inelastic behavior of ductile metals, a systematic macroscopic framework is established for describing the coupled process of elastic, plastic and damage deformations of anisotropic nature. Based on the concepts of continuum damage mechanics constitutive equations for ductile engineering materials are discussed in this paper by introducing a limited number of state parameters. Damage evolution equations are derived in terms of appropriate stress tensors providing a more realistic physical representation of material degradation. Thus, a general anisotropic damage evolution model is proposed and satisfactorily verified by experimental determination of damage variables. These efforts lead to proper understanding and appropriate mechanical description of the damage processes of some technologically important materials caused by internal defects which are of importance in discussing the mechanical effects of the material damage on the macroscopic behavior of ductile materials as well as in elucidating the process leading from these defects to final fracture. Briefly, the present anisotropic elastic–plastic–damage framework which involves the constitutive equations of elasticity, plasticity and damage provides a comprehensive theory of anisotropic continuum damage mechanics capable of solving practical engineering problems. It is based on

the introduction of metric transformation tensors. The kinematic description employs the consideration of damaged as well as fictitious undamaged configurations and, therefore, the model does not need strain equivalence, stress equivalence or strain energy equivalence approaches often used in continuum damage theories to be able to connect matrix material and aggregate variables. The damaged and corresponding undamaged configurations are related via metric transformations which allow for the interpretation of damage tensors representing material degradation and induced elastic anisotropy. Therefore, a characteristic feature of the proposed model is the kinematic description of anisotropic damage. The modular structure is accomplished by the kinematic decomposition of strain rates into elastic, plastic and damage parts which take into account the physics of these deformation processes. To be able to address equally the two physically distinct modes of irreversible changes, i.e. plastic flow and damage, free energy functions with respect to the fictitious undamaged configuration as well as to the current damaged configuration are introduced separately. A generalized macroscopic yield condition based on invariants of the effective stress tensor is used to adequately describe the plastic flow properties of ductile metals observed experimentally. The evolution of the effective plastic part of the strain rate tensor is determined via a non-associated flow rule. With respect to the damaged configurations the concept of a damage surface formulated in terms of stress components referred to the elastically unloaded (stress free) damaged configuration is used to designate the onset and subsequent evolution of damage. In addition, damage potentials in terms of these stresses are introduced and the constitutive expressions for damage strain rates are established. The damage strain rate tensor takes into account isotropic as well as anisotropic effects providing a realistic physical representation of material degradation. Identification of material parameters is discussed in some detail. The applicability of the present continuum damage theory is demonstrated by numerical simulation of the inelastic damage process of specimens manufactured of various technologically important materials undergoing tensile loading. Comparison of numerical results with experimental data demonstrate the efficiency of the proposed continuum damage model.

2. Kinematics

The macroscopic kinematic framework presented by Brünig (2001) is used to describe the inelastic deformations including anisotropic damage by microdefects. Briefly, the continuous body in the initial undeformed configuration $\overset{o}{\mathcal{B}}$, which may have an initial damage in the material, is shown in Fig. 1. Tensorial quantities referred to this configuration are formulated using the base vectors $\overset{o}{\mathbf{g}}_i$ and the associated metric coefficients are given by $\overset{o}{G}_{ij} = \overset{o}{\mathbf{g}}_i \cdot \overset{o}{\mathbf{g}}_j$. In addition, the current elastic-plastically deformed and damaged configuration $\mathcal{B}$ is considered and the corresponding base vectors and metric coefficients are $\mathbf{g}_i$ and $G_{ij} = \mathbf{g}_i \cdot \mathbf{g}_j$, respectively (see Fig. 1). All actual quantities are referred to this current damaged configuration.

The kinematic theory for the mechanics of large deformations of solids is based on the metric transformation tensor

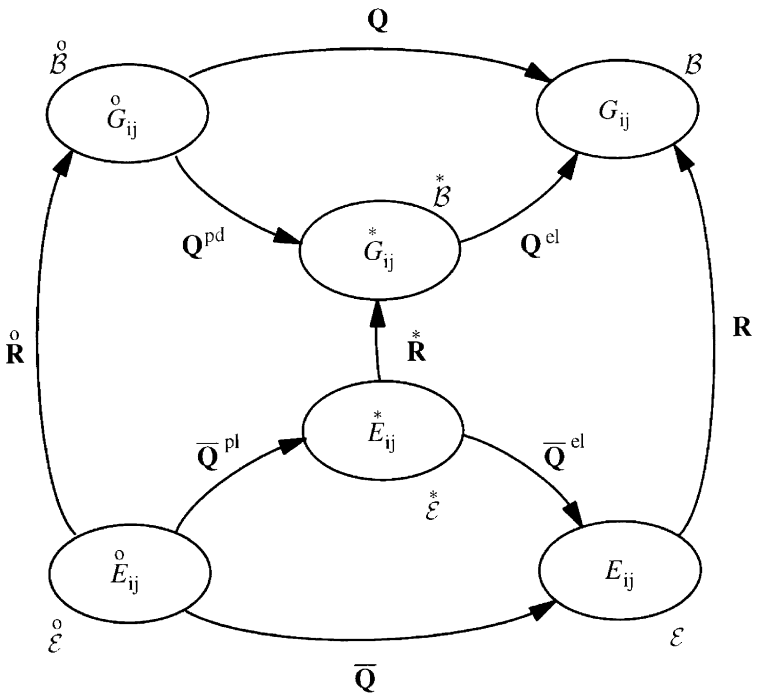

Fig. 1. Configurations, metrics, and metric transformation tensors.

$$\mathbf{Q} = Q^{i}_{\ j}\mathbf{g}_i \otimes \mathbf{g}^j = \overset{o}{G}{}^{ik}\ G_{kj}\mathbf{g}_i \otimes \mathbf{g}^j = \mathbf{B}\ \ \mathbf{G} \tag{1}$$

which has also been used by Lehmann (1989, 1991) and by Brünig (2001). In Eq. (1) $\mathbf{Q}$ represents the mixed-variant counterpart of the Finger tensor $\mathbf{B}=\mathbf{F}\mathbf{F}^T=\mathbf{V}^2$ often used in finite strain formulations, where $\mathbf{F}$ denotes the usual deformation gradient and $\mathbf{V}$ the left-hand stretch tensor, and $\mathbf{G}=G_{ij}\mathbf{g}^i \otimes \mathbf{g}^j$ is the metric tensor of the current damaged configuration $\mathcal{B}$. This leads to the definition of the logarithmic Hencky strain tensor

$$\mathbf{A} = \frac{1}{2}\ln\mathbf{Q} = \frac{1}{2}(\ln Q)^{i}_{\ j}\mathbf{g}_i \otimes \mathbf{g}^j = A^{i}_{\ .j}\mathbf{g}_i \otimes \mathbf{g}^j. \tag{2}$$

In addition, the nonsymmetric objective Oldroyd rate of the metric transformation tensor (1)

$$\dot{\mathbf{Q}} = \overset{o}{G}{}^{ik}\dot{G}_{kj}\mathbf{g}_i \otimes \mathbf{g}^j \tag{3}$$

is used to define the symmetric strain rate

$$\dot{\mathbf{H}} = \frac{1}{2}\mathbf{Q}^{-1}\dot{\mathbf{Q}} = \frac{1}{2}G^{ik}\dot{G}_{kj}\mathbf{g}_i \otimes \mathbf{g}^j = \dot{H}^{i}_{\ .j}\mathbf{g}_i \otimes \mathbf{g}^j \tag{4}$$

which may be seen as the mixed-variant counterpart of the Oldroyd rate of the well-known Almansi strain tensor.

Furthermore, the macroscopic formulation of the large deformation behavior of damaged elastic–plastic materials is based on the multiplicative decomposition of the metric transformation tensor

$$\mathbf{Q} = \mathbf{Q}^{\mathrm{pd}}\mathbf{Q}^{\mathrm{el}} \tag{5}$$

into its respective inelastic (plastic and damage) part

$$\mathbf{Q}^{\mathrm{pd}} = \overset{o}{G}{}^{ik} G_{kj}\mathbf{g}_i * \mathbf{g}_i \otimes \mathbf{g}^j \tag{6}$$

and its elastic part

$$\mathbf{Q}^{\mathrm{el}} = \overset{*}{G}{}^{ik} G_{kj}\mathbf{g}_i \otimes \mathbf{g}^j. \tag{7}$$

In Eqs. (6) and (7) $\overset{*}{G}_{ij}$ denotes the metric of the base vectors of the intermediate configuration $\overset{*}{\mathcal{B}}$ which represents a fictitious unstressed state at fixed values of internal variables (see Fig. 1). To be able to compute reversible deformations the elastic Hencky strain tensor

$$\mathbf{A}^{\mathrm{el}} = \frac{1}{2}\ln\mathbf{Q}^{\mathrm{el}} \tag{8}$$

is introduced. These elastic strains are assumed to be kinematically independent from accompanying inelastic deformations. Using, now, the multiplicative decomposition of the metric transformation tensor (5), the proposed strain rate tensor (4) is rewritten in the form

$$\dot{\mathbf{H}} = \frac{1}{2}\mathbf{Q}^{\mathrm{el}-1}\mathbf{Q}^{\mathrm{pd}-1}\dot{\mathbf{Q}}^{\mathrm{pd}}\mathbf{Q}^{\mathrm{el}} + \frac{1}{2}\mathbf{Q}^{\mathrm{el}-1}\dot{\mathbf{Q}}^{\mathrm{el}} = \dot{\mathbf{H}}^{\mathrm{pd}} + \dot{\mathbf{H}}^{\mathrm{el}} \tag{9}$$

which leads to the additive decomposition of the elastic and inelastic strain rates

$$\dot{\mathbf{H}}^{\mathrm{el}} = \frac{1}{2}\mathbf{Q}^{\mathrm{el}-1}\dot{\mathbf{Q}}^{\mathrm{el}} \tag{10}$$

and

$$\dot{\mathbf{H}}^{\mathrm{pd}} = \frac{1}{2}\mathbf{Q}^{-1}\dot{\mathbf{Q}}^{\mathrm{pd}}\mathbf{Q}^{\mathrm{el}}, \tag{11}$$

respectively.

Dislocations, microvoids and microcracks are the most common modes of irreversible microstructural deformations at each stage of the loading process. In particular, pure plastic flow develops by dislocation motion and sliding phenomena along some preferential crystallographic planes whereas damage-related irreversible deformations are due to residual opening of microdefects after unloading. These dissipative processes are distinctly different in their nature and in the manner in which they affect the compliance of the material. Consequently, for damage-coupled

elastic–plastic theories two sets of internal variables characterizing formation of dislocations (plastic internal variables) as well as describing nucleation and propagation of microdefects (damage internal variables) are separately used to adequately describe the constitutive behavior and to compute the corresponding strain rate tensors.

Following Brünig (2001), the central idea of the present framework is the introduction of specific metric coefficients as appropriate measures of evolving damage. Therefore, similar to the theories presented by Betten (1982, 1983), Murakami (1988), Grabacki (1991), and Voyiadjis and Park (1999), effective undamaged configurations are introduced which characterize the fictitious undamaged material behavior based on standard terminology of nonlinear continuum mechanics. Thus, the model does not need strain equivalence, stress equivalence or strain energy equivalence approaches often used in continuum damage theories to be able to connect matrix material and aggregate variables, see e.g. Lemaitre (1985a,b), Chow and Wang (1987), Simo and Ju (1987), and Voyiadjis and Kattan (1992) among many others. As can be seen in Fig. 1 undamaged configurations are defined which are obtained by fictitiously removing all the damage the body has undergone. In particular, the current fictitious configuration $\mathcal{E}$ of the body is obtained from the actual damaged configuration $\mathcal{B}$ by fictitiously removing all the damage of the deformed body. The corresponding base vectors and metric coefficients of the current undamaged configuration are given by $\mathbf{e}_i$ and $E_{ij}=\mathbf{e}_i\cdot\mathbf{e}_j$, respectively. In addition, the initial undeformed body $\overset{o}{\mathcal{B}}$ may have a pre-existing damage state. The corresponding initial undamaged configuration $\overset{o}{\mathcal{E}}$ with base vectors $\overset{o}{\mathbf{e}}_i$ and metric coefficients $\overset{o}{E}_{ij}=\overset{o}{\mathbf{e}}_i\cdot\overset{o}{\mathbf{e}}_j$ is obtained by fictitiously removing the initial damage from the undeformed but initially damaged configuration $\overset{o}{\mathcal{B}}$.

To be able to describe the kinematics of undamaged configurations, the undamaged metric transformation tensor

$$\bar{\mathbf{Q}}_{\mathbf{u}}=\bar{Q}^{i}_{\ .j}\ \mathbf{e}_i\otimes\mathbf{e}^j=\overset{o}{E}^{ik}E_{kj}\ \mathbf{e}_i\otimes\mathbf{e}^j \tag{12}$$

is introduced which—similar to the kinematics discussed above—leads to the definition of the corresponding undamaged logarithmic strain tensor

$$\bar{\mathbf{A}}_{\mathbf{u}}=\frac{1}{2}\ln\bar{\mathbf{Q}}_{\mathbf{u}}=\frac{1}{2}\left(\ln\bar{Q}\right)^{i}_{\ .j}\mathbf{e}_i\otimes\mathbf{e}^j=\bar{A}^{i}_{\ .j}\ \mathbf{e}_i\otimes\mathbf{e}^j \tag{13}$$

as well as to the undamaged strain rate tensor

$$\dot{\bar{\mathbf{H}}}_{\mathbf{u}}=\frac{1}{2}\bar{\mathbf{Q}}_{\mathbf{u}}^{-1}\dot{\bar{\mathbf{Q}}}_{\mathbf{u}}, \tag{14}$$

where the nonsymmetric Oldroyd type rate of the metric transformation tensor $\dot{\bar{\mathbf{Q}}}_{\mathbf{u}}=\overset{o}{E}^{ik}\ \dot{E}_{kj}\ \mathbf{e}_i\otimes\mathbf{e}^j$ has been used. As can be seen from Fig. 1, the undamaged metric transformation tensor

$$\bar{\mathbf{Q}}_{\mathbf{u}}=\bar{\mathbf{Q}}_{\mathbf{u}}^{\mathrm{pl}}\bar{\mathbf{Q}}_{\mathbf{u}}^{\mathrm{el}} \tag{15}$$

is multiplicatively decomposed into its plastic part

$$\bar{\mathbf{Q}}_{\mathbf{u}}^{\mathrm{pl}} = \overset{o}{E}^{ik}\overset{*}{E}_{kj}\ \mathbf{e}_i \otimes \mathbf{e}^j \tag{16}$$

and into its elastic part

$$\bar{\mathbf{Q}}_{\mathbf{u}}^{\mathrm{el}} = \overset{*}{E}^{ik}E_{kj}\ \mathbf{e}_i \otimes \mathbf{e}^j. \tag{17}$$

The symmetric undamaged elastic metric transformation tensor $\bar{\mathbf{Q}}_{\mathbf{u}}^{\mathrm{el}}$ describes elastic stretching of the matrix material and is used to introduce the logarithmic undamaged elastic strain tensor

$$\bar{\mathbf{A}}_{\mathbf{u}}^{\mathrm{el}} = \frac{1}{2}\ln\bar{\mathbf{Q}}_{\mathbf{u}}^{\mathrm{el}}. \tag{18}$$

The plastic part of the undamaged metric transformation tensor $\bar{\mathbf{Q}}_{\mathbf{u}}^{\mathrm{pl}}$, on the other hand, is arising from purely irreversible processes due to dislocation motions in the matrix material. In addition, Eqs. (14) and (15) lead to the additive decomposition of the undamaged strain rate tensor

$$\dot{\bar{\mathbf{H}}}_{\mathbf{u}} = \frac{1}{2}\bar{\mathbf{Q}}_{\mathbf{u}}^{\mathrm{el}-1}\bar{\mathbf{Q}}_{\mathbf{u}}^{\mathrm{pl}-1}\dot{\bar{\mathbf{Q}}}_{\mathbf{u}}^{\mathrm{pl}}\bar{\mathbf{Q}}_{\mathbf{u}}^{\mathrm{el}} + \frac{1}{2}\bar{\mathbf{Q}}_{\mathbf{u}}^{\mathrm{el}-1}\dot{\bar{\mathbf{Q}}}_{\mathbf{u}}^{\mathrm{el}} = \dot{\bar{\mathbf{H}}}_{\mathbf{u}}^{\mathrm{pl}} + \dot{\bar{\mathbf{H}}}_{\mathbf{u}}^{\mathrm{el}}, \tag{19}$$

where the undamaged elastic and plastic strain rate tensors are defined as

$$\dot{\bar{\mathbf{H}}}_{\mathbf{u}}^{\mathrm{el}} = \frac{1}{2}\bar{\mathbf{Q}}_{\mathbf{u}}^{\mathrm{el}-1}\dot{\bar{\mathbf{Q}}}_{\mathbf{u}}^{\mathrm{el}}, \tag{20}$$

and

$$\dot{\bar{\mathbf{H}}}_{\mathbf{u}}^{\mathrm{pl}} = \frac{1}{2}\bar{\mathbf{Q}}_{\mathbf{u}}^{-1}\dot{\bar{\mathbf{Q}}}_{\mathbf{u}}^{\mathrm{pl}}\bar{\mathbf{Q}}_{\mathbf{u}}^{\mathrm{el}}, \tag{21}$$

respectively.

Moreover, using the damage deformation gradient

$$\tilde{\mathbf{F}} = \mathbf{g}_i \otimes \mathbf{e}^i \tag{22}$$

the undamaged kinematic variables (12)–(21) can be transformed to the current damaged configuration $\mathcal{B}$. In particular, the effective metric transformation tensor is then given by

$$\bar{\mathbf{Q}} = \tilde{\mathbf{F}}\bar{\mathbf{Q}}_{\mathbf{u}}\tilde{\mathbf{F}}^{-1} = \bar{Q}^i_{\ j}\mathbf{g}_i \otimes \mathbf{g}^j. \tag{23}$$

the effective strain tensor is

$$\bar{\mathbf{A}} = \tilde{\mathbf{F}}\bar{\mathbf{A}}_{\mathbf{u}}\tilde{\mathbf{F}}^{-1} = \bar{A}^i_{\ j}\mathbf{g}_i \otimes \mathbf{g}^j \tag{24}$$

and their effective elastic and plastic counterparts can be expressed as

$$\bar{\mathbf{Q}}^{\mathrm{el}} = \tilde{\mathbf{F}}\bar{\mathbf{Q}}_{\mathbf{u}}^{\mathrm{el}}\tilde{\mathbf{F}}^{-1} = \overset{*}{E}^{ik}E_{kj}\mathbf{g}_i \otimes \mathbf{g}^j, \tag{25}$$

$$\bar{\mathbf{Q}}^{\mathrm{pl}} = \tilde{\mathbf{F}}\bar{\mathbf{Q}}_{\mathbf{u}}^{\mathrm{pl}}\tilde{\mathbf{F}}^{-1} = \overset{\circ}{E}^{ik}\overset{*}{E}_{kj}\mathbf{g}_i \otimes \mathbf{g}^j, \tag{26}$$

and

$$\bar{\mathbf{A}}^{\mathrm{el}} = \tilde{\mathbf{F}}\bar{\mathbf{A}}_{\mathbf{u}}^{\mathrm{el}}\tilde{\mathbf{F}}^{-1} = \left(\bar{A}^{\mathrm{el}}\right)^{i}_{.j}\mathbf{g}_i \otimes \mathbf{g}^j. \tag{27}$$

In addition, the corresponding objective Oldroyd type rate tensors can be written in the form

$$\overset{\cdot}{\bar{\mathbf{Q}}} = \tilde{\mathbf{F}}\overset{\cdot}{\bar{\mathbf{Q}}}_{\mathbf{u}}\tilde{\mathbf{F}}^{-1} = \overset{\cdot}{\bar{Q}}{}^{i}_{.j}\ \mathbf{g}_i \otimes \mathbf{g}^j, \tag{28}$$

$$\overset{\cdot}{\bar{\mathbf{Q}}}^{\mathrm{el}} = \tilde{\mathbf{F}}\overset{\cdot}{\bar{\mathbf{Q}}}_{\mathbf{u}}^{\mathrm{el}}\tilde{\mathbf{F}}^{-1} = \left(\overset{\cdot}{\bar{Q}}{}^{\mathrm{el}}\right)^{i}_{.j}\mathbf{g}_i \otimes \mathbf{g}^j, \tag{29}$$

and

$$\overset{\cdot}{\bar{\mathbf{Q}}}^{\mathrm{pl}} = \tilde{\mathbf{F}}\overset{\cdot}{\bar{\mathbf{Q}}}_{\mathbf{u}}^{\mathrm{pl}}\tilde{\mathbf{F}}^{-1} = \left(\overset{\cdot}{\bar{Q}}{}^{\mathrm{pl}}\right)^{i}_{.j}\mathbf{g}_i \otimes \mathbf{g}^j, \tag{30}$$

as well as

$$\overset{\cdot}{\bar{\mathbf{H}}} = \tilde{\mathbf{F}}\overset{\cdot}{\bar{\mathbf{H}}}_{\mathbf{u}}\tilde{\mathbf{F}}^{-1} = \overset{\cdot}{\bar{H}}{}^{i}_{.j}\ \mathbf{g}_i \otimes \mathbf{g}^j, \tag{31}$$

$$\overset{\cdot}{\bar{\mathbf{H}}}^{\mathrm{el}} = \tilde{\mathbf{F}}\overset{\cdot}{\bar{\mathbf{H}}}_{\mathbf{u}}^{\mathrm{el}}\tilde{\mathbf{F}}^{-1} = \left(\overset{\cdot}{\bar{H}}{}^{\mathrm{el}}\right)^{i}_{.j}\mathbf{g}_i \otimes \mathbf{g}^j, \tag{32}$$

and

$$\overset{\cdot}{\bar{\mathbf{H}}}^{\mathrm{pl}} = \tilde{\mathbf{F}}\overset{\cdot}{\bar{\mathbf{H}}}_{\mathbf{u}}^{\mathrm{pl}}\tilde{\mathbf{F}}^{-1} = \left(\overset{\cdot}{\bar{H}}{}^{\mathrm{pl}}\right)^{i}_{.j}\mathbf{g}_i \otimes \mathbf{g}^j. \tag{33}$$

Furthermore, following Brünig (2001), the kinematics of damage will be explicitly characterized by metric transformations and corresponding logarithmic strain measures. Therefore, the simultaneous motion of the real body and the fictitious undamaged one will be considered, and as can be seen from Fig. 1, the second order tensors

$$\overset{o}{\mathbf{R}} = \overset{o}{R}{}^{i}_{.j}\mathbf{g}_i \otimes \mathbf{g}^j = \overset{o}{E}{}^{ik}\overset{o}{G}_{kj}\mathbf{g}_i \otimes \mathbf{g}^j, \tag{34}$$

$$\overset{*}{\mathbf{R}} = \overset{*}{R}{}^{i}_{.j}\mathbf{g}_i \otimes \mathbf{g}^j = \overset{*}{E}{}^{ik}\overset{*}{G}_{kj}\mathbf{g}_i \otimes \mathbf{g}^j \tag{35}$$

and

$$\mathbf{R} = R^{i}_{.j}\ \mathbf{g}_i \otimes \mathbf{g}^j = E^{ik} G_{kj} \mathbf{g}_i \otimes \mathbf{g}^j \tag{36}$$

are introduced as metric transformation tensors between the respective damaged and undamaged configurations. In particular, the initial damage tensor $\overset{o}{\mathbf{R}}$ characterizes the pre-existing damage state, and $\mathbf{R}$ and $\overset{*}{\mathbf{R}}$ represent internal state variables which describe the current general anisotropic damage state of the material. Note that in the current damaged configuration $\mathcal{B}$ the material is subjected to damage and macroscopic elastic–plastic deformation at the same time. Thus, the current damage tensor $\mathbf{R}$ defined by Eq. (36) also depends on the current state of deformation. This means that the tensor $\mathbf{R}$ can not properly describe the internal state of damage in the case of moderate or large elastic deformations. However, concerning the damage state of the material element in the current configuration $\mathcal{B}$ only the irreversible change of internal structure caused by the deformation process from $\overset{o}{\mathcal{B}}$ to $\mathcal{B}$ is essential. Following Murakami (1988), the tensor $\overset{*}{\mathbf{R}}$, which relates the elastically unloaded configuration $\overset{*}{\mathcal{B}}$ and the corresponding fictitious elastically unloaded and undamaged configuration $\overset{*}{\mathcal{E}}$, characterizes the actual damage state of the current configuration independently of the current elastic deformation. Therefore, to be able to unequivocally define appropriate damage variables, they have to be defined in the stress-free configuration. Consequently, damage states are identified by the damage tensor $\overset{*}{\mathbf{R}}$ which is used to define the corresponding logarithmic damage strain tensor

$$\mathbf{A}^{\mathrm{da}} = \frac{1}{2} \ln \overset{*}{\mathbf{R}}. \tag{37}$$

Note that this damage strain tensor describes the complete material deterioration the body has undergone including the initial damage described by $\overset{o}{\mathbf{R}}$. As may be seen in Fig. 1, the relation between the current damage tensors $\mathbf{R}$ and $\overset{*}{\mathbf{R}}$ is given by

$$\mathbf{R} = \bar{\mathbf{Q}}^{\mathrm{el}-1}\ \overset{*}{\mathbf{R}}\ \ \mathbf{Q}^{\mathrm{el}} \tag{38}$$

and the metric transformation tensor $\mathbf{Q}$ can be multiplicatively decomposed as

$$\mathbf{Q} = \overset{o}{\mathbf{R}}{}^{-1} \bar{\mathbf{Q}}^{\mathrm{pl}}\ \overset{*}{\mathbf{R}}\ \mathbf{Q}^{\mathrm{el}}, \tag{39}$$

Then, the completely different physical counterparts are now kinematically decomposed. This allows separate formulation of the corresponding constitutive laws. In addition, making use of Eqs. (10), (25), (26), (30), (38), and (39) the strain rate tensor (4) can be rewritten in the form

$$\dot{\mathbf{H}} = \dot{\mathbf{H}}^{\mathrm{el}} + \mathbf{R}^{-1} \dot{\bar{\mathbf{H}}}^{\mathrm{pl}} \mathbf{R} + \mathbf{Q}^{\mathrm{el}-1} \dot{\mathbf{H}}^{\mathrm{da}} \mathbf{Q}^{\mathrm{el}} \tag{40}$$

with the damage strain rate

$$\dot{\mathbf{H}}^{\mathrm{da}} = \frac{1}{2}\overset{*}{\mathbf{R}}^{-1}\dot{\overset{*}{\mathbf{R}}}. \tag{41}$$

Moreover, it is assumed that the intermediate and the current undamaged configurations, $\overset{*}{\mathcal{E}}$ and $\mathcal{E}$, are related in the same way as the intermediate and current damaged configurations, $\overset{*}{\mathcal{B}}$ and $\mathcal{B}$ (see e.g. Murakami, 1988; Brünig, 2001). As a result, these undamaged and damaged configurations are subjected to the identical elastic metric transformation

$$\mathbf{Q}^{\mathrm{el}} = \bar{\mathbf{Q}}^{\mathrm{el}}, \tag{42}$$

which is a common assumption in homogenization theories. This leads to the equivalence of the elastic strain tensors

$$\mathbf{A}^{\mathrm{el}} = \frac{1}{2}\ln\mathbf{Q}^{\mathrm{el}} = \frac{1}{2}\ln\bar{\mathbf{Q}}^{\mathrm{el}} = \bar{\mathbf{A}}^{\mathrm{el}} \tag{43}$$

and the elastic strain rates

$$\dot{\mathbf{H}}^{\mathrm{el}} = \dot{\bar{\mathbf{H}}}^{\mathrm{el}}. \tag{44}$$

3. Thermodynamics

3.1. Definition of stress tensors

To be able to formulate constitutive equations, appropriate stress measures are introduced considering the damaged and undamaged configurations, respectively. Usually, the current stress state of the actual deformed and damaged configuration $\mathcal{B}$ will be adequately described by the Kirchhoff stress tensor

$$\mathbf{T} = T^{i}_{\cdot j}\,\mathbf{g}_i \otimes \mathbf{g}^j. \tag{45}$$

In addition, in the fictitious undamaged configuration the mechanical effect of the Kirchhoff stress tensor $\mathbf{T}$ (45) is described by the effective stress tensor

$$\mathbf{S} = S^{i}_{\cdot j}\mathbf{e}_i \otimes \mathbf{e}^j. \tag{46}$$

The symmetric tensor $\mathbf{S}$ is a fictitious stress measure which represents the magnified effect of stress due to damage. Furthermore, using Eq. (22) the effective stresses can be formulated with respect to the base vectors of the current damaged configuration $\mathcal{B}$

$$\bar{\mathbf{T}} = \tilde{\mathbf{F}}\mathbf{S}\tilde{\mathbf{F}}^{-1} = S^{i}_{\cdot j}\,\mathbf{g}_i \otimes \mathbf{g}^j. \tag{47}$$

3.2. Effective undamaged configurations

Considering the undamaged configurations, the rate of the effective specific mechanical work $\dot{\bar{w}}$ is defined by

$$\rho_o \dot{\bar{w}} = \bar{\mathbf{T}} \cdot \dot{\bar{\mathbf{H}}} \tag{48}$$

where ρ_o denotes the initial mass density. Using Eqs. (19) and (31)–(33), the rate of effective mechanical work (48) can be additively decomposed according to

$$\rho_o \dot{\bar{w}} = \rho_o \dot{\bar{w}}^{\mathrm{el}} + \rho_o \dot{\bar{w}}^{\mathrm{pl}} = \bar{\mathbf{T}} \cdot \dot{\bar{\mathbf{H}}}^{\mathrm{el}} + \bar{\mathbf{T}} \cdot \dot{\bar{\mathbf{H}}}^{\mathrm{pl}} \tag{49}$$

into an effective elastic part $\dot{\bar{w}}^{\mathrm{el}}$ governed by thermodynamic state equations as well as into an effective plastic part $\dot{\bar{w}}^{\mathrm{pl}}$.

Moreover, the effective specific free energy $\bar{\phi}$ of the fictitious undamaged configurations is introduced. Since the effective elastic behavior of the matrix material is not influenced by the hardening state, $\bar{\phi}$ is assumed to be additively decomposed into an effective elastic and an effective plastic part

$$\bar{\phi} = \bar{\phi}^{\mathrm{el}}\left(\bar{\mathbf{A}}^{\mathrm{el}}\right) + \bar{\phi}^{\mathrm{pl}}(\gamma) \tag{50}$$

where γ denotes an internal mechanical state variable characterizing plastic deformation behavior. Then, the second law of thermodynamics (Clausius–Duhem inequality) can be written in the form

$$\dot{\bar{w}} - \dot{\bar{\phi}} \geqslant 0. \tag{51}$$

Making use of Eqs. (49) and (50) one arrives at

$$\bar{\mathbf{T}} \cdot \dot{\bar{\mathbf{H}}}^{\mathrm{el}} + \bar{\mathbf{T}} \cdot \dot{\bar{\mathbf{H}}}^{\mathrm{pl}} - \rho_o \frac{\partial \bar{\phi}^{\mathrm{el}}}{\partial \bar{\mathbf{A}}^{\mathrm{el}}} \cdot \dot{\bar{\mathbf{A}}}^{\mathrm{el}} - \rho_o \dot{\bar{\phi}}^{\mathrm{pl}} \geqslant 0. \tag{52}$$

Considering non-dissipative processes in the effective elastic range Eq. (52) leads to the relation

$$\bar{\mathbf{T}} \cdot \dot{\bar{\mathbf{H}}}^{\mathrm{el}} - \rho_o \frac{\partial \bar{\phi}^{\mathrm{el}}}{\partial \bar{\mathbf{A}}^{\mathrm{el}}} \cdot \dot{\bar{\mathbf{A}}}^{\mathrm{el}} = 0. \tag{53}$$

Using Eqs. (25), (29) and (32), Eq. (48) can be rewritten in the form

$$\bar{\mathbf{T}} \cdot \frac{1}{2} \bar{\mathbf{Q}}^{\mathrm{el}-1} \dot{\bar{\mathbf{Q}}}^{\mathrm{el}} = \rho_o \frac{\partial \bar{\phi}^{\mathrm{el}}}{\partial \bar{\mathbf{A}}^{\mathrm{el}}} \frac{\partial \bar{\mathbf{A}}^{\mathrm{el}}}{\partial \bar{\mathbf{Q}}^{\mathrm{el}}} \cdot \dot{\bar{\mathbf{Q}}}^{\mathrm{el}} \tag{54}$$

which yields the thermic state equation

$$\bar{\mathbf{T}} = \rho_o \left(\frac{\partial \bar{\phi}^{\mathrm{el}}}{\partial \bar{\mathbf{A}}^{\mathrm{el}}} \frac{\partial \bar{\mathbf{A}}^{\mathrm{el}}}{\partial \bar{\mathbf{Q}}^{\mathrm{el}}} \bar{\mathbf{Q}}^{\mathrm{el}} + \bar{\mathbf{Q}}^{\mathrm{el}} \frac{\partial \bar{\mathbf{A}}^{\mathrm{el}}}{\partial \bar{\mathbf{Q}}^{\mathrm{el}}} \frac{\partial \bar{\phi}^{\mathrm{el}}}{\partial \bar{\mathbf{A}}^{\mathrm{el}}} \right) \tag{55}$$

governing strictly reversible deformations. Following Lehmann (1989) this leads in the case of isotropic elastic matrix material behavior and taking into account the logarithmic elastic strain tensor (18) and (27) to the simple relations

$$\bar{\mathbf{T}} = \rho_o \frac{\partial \bar{\phi}^{\mathrm{el}}}{\partial \bar{\mathbf{A}}^{\mathrm{el}}} \tag{56}$$

and

$$\bar{\mathbf{T}} \cdot \dot{\bar{\mathbf{H}}}^{\mathrm{el}} = \bar{\mathbf{T}} \cdot \dot{\bar{\mathbf{A}}}^{\mathrm{el}}. \tag{57}$$

Then, Eq. (52) reduces to the effective dissipation function $\bar{D}$ which is assumed to obey the Kelvin inequality

$$\bar{D} = \bar{\mathbf{T}} \cdot \dot{\bar{\mathbf{H}}}^{\mathrm{pl}} - \rho_o \dot{\bar{\phi}}^{\mathrm{pl}} \geqslant 0. \tag{58}$$

As a result, the evolution equation for the effective plastic part of the deformation will be formulated in terms of $\bar{\mathbf{H}}^{\mathrm{pl}}$.

3.3. Anisotropically damaged configurations

The finite elastic–plastic deformation behavior including anisotropic damage is also viewed within the framework of thermodynamics with internal state variables. The experimentally observed nonlinearities in ductile metal behavior are well documented in the literature and arise from two distinct microstructural changes that take place in the material: one is the plastic flow, the other is the development of microvoids and microcracks. Especially, plastic flow results in permanent deformation and is the consequence of dislocation processes along preferred slip planes which are predominantly controlled by the presence of local shear stresses (see e.g. Asaro, 1983). Since the crystal lattice has been shown to be unaffected during the slip process, the elastic compliances remain insensitive to this mode of microstructural changes. On the other hand, microcracking destroys the band between material grains. It also results in permanent deformation but in contrast to the plastic material behavior it affects the elastic properties. As a consequence, the elastic properties depend on damage variables but not on plastic strains which leads to the assumption of uncoupled elasticity and plasticity. In addition, as has been proposed by Lemaitre (1985a) and Lu and Chow (1990) among others, it is postulated that the energies involved in plastic flow and damage processes are independent. Thus, taking into account Eq. (40), the rate of the specific mechanical work

$$\rho_o \ \dot{w} = \mathbf{T} \cdot \dot{\mathbf{H}} \tag{59}$$

is additively decomposed:

$$\rho_o \dot{w} = \rho_o \dot{w}^{\mathrm{el}} + \rho_o \dot{w}^{\mathrm{pl}} + \rho_o \dot{w}^{\mathrm{da}}$$
$$= \mathbf{T}\cdot\dot{\mathbf{H}}^{\mathrm{el}} + \mathbf{T}\cdot\left(\mathbf{R}^{-1}\ \dot{\bar{\mathbf{H}}}^{\mathrm{pl}}\ \mathbf{R}\right) + \mathbf{T}\cdot\left(\mathbf{Q}^{\mathrm{el}-1}\ \dot{\mathbf{H}}^{\mathrm{da}}\ \mathbf{Q}^{\mathrm{el}}\right). \tag{60}$$

Furthermore, the Helmholtz free energy of the damaged material sample is assumed to consist of three parts:

$$\phi = \phi^{\mathrm{el}}\left(\mathbf{A}^{\mathrm{el}}, \mathbf{A}^{\mathrm{da}}\right) + \phi^{\mathrm{pl}}(\gamma) + \phi^{\mathrm{da}}(\mu). \tag{61}$$

Namely, the free energy ϕ^{el} is used to describe the elastic response of the damaged material at the current state of deformation and material damage, and the energies ϕ^{pl} and ϕ^{da} are exclusively related to plastic flow and damage development, respectively, where μ denotes an internal mechanical state variable characterizing damage deformation behavior. The free energy due to plastic deformations is usually small in comparison with the elastic counterpart and, therefore, the effects of damage on the plastic part will be neglected. In addition, the influence of other state variables on these free energies are assumed to be small. Hence, it is postulated that the energies involved in plastic flow and damage processes are independent. In particular, the elastic part of the free energy of the damaged material ϕ^{el} should now be expressed in terms of the logarithmic elastic and damage strain tensors (8) and (37), whereas the plastic part, ϕ^{pl}, due to plastic hardening, and the damaged part, ϕ^{da}, due to damage strengthening, only take into account the internal state variables, γ and μ. Making use of Eqs. (60) and (61) the second law of thermodynamics can then be written in the form

$$\rho_o\ \dot{w} - \rho_o\ \dot{\phi} = \mathbf{T}\cdot\dot{\mathbf{H}}^{\mathrm{el}} + \left(\mathbf{R}\ \mathbf{T}\ \mathbf{R}^{-1}\right)\cdot\dot{\bar{\mathbf{H}}}^{\mathrm{pl}} + \left(\mathbf{Q}^{\mathrm{el}}\ \mathbf{T}\ \mathbf{Q}^{\mathrm{el}-1}\right)\cdot\dot{\mathbf{H}}^{\mathrm{da}}$$
$$- \rho_o \frac{\partial\phi^{\mathrm{el}}}{\partial\mathbf{A}^{\mathrm{el}}}\cdot\dot{\mathbf{A}}^{\mathrm{el}} - \rho_o \frac{\partial\phi^{\mathrm{el}}}{\partial\mathbf{A}^{\mathrm{da}}}\cdot\dot{\mathbf{A}}^{\mathrm{da}} - \rho_o\,\dot{\phi}^{\mathrm{pl}}(\gamma) - \rho_o\,\dot{\phi}^{\mathrm{da}}(\mu) \geqslant 0. \tag{62}$$

Considering non-dissipative processes in the elastic range, Eq. (62) leads to the relation

$$\mathbf{T}\cdot\dot{\mathbf{H}}^{\mathrm{el}} - \rho_o \frac{\partial\phi^{\mathrm{el}}}{\partial\mathbf{A}^{\mathrm{el}}}\cdot\dot{\mathbf{A}}^{\mathrm{el}} = 0 \tag{63}$$

and making use of Eq. (10) one gets

$$\mathbf{T}\cdot\frac{1}{2}\mathbf{Q}^{\mathrm{el}-1}\dot{\mathbf{Q}}^{\mathrm{el}} = \rho_o \frac{\partial\phi^{\mathrm{el}}}{\partial\mathbf{A}^{\mathrm{el}}}\frac{\partial\mathbf{A}^{\mathrm{el}}}{\partial\mathbf{Q}^{\mathrm{el}}}\cdot\dot{\mathbf{Q}}^{\mathrm{el}} \tag{64}$$

which yields the thermic state equation

$$\mathbf{T} = \rho_o\left(\frac{\partial\phi^{\mathrm{el}}}{\partial\mathbf{A}^{\mathrm{el}}}\frac{\partial\mathbf{A}^{\mathrm{el}}}{\partial\mathbf{Q}^{\mathrm{el}}}\mathbf{Q}^{\mathrm{el}} + \mathbf{Q}^{\mathrm{el}}\frac{\partial\mathbf{A}^{\mathrm{el}}}{\partial\mathbf{Q}^{\mathrm{el}}}\frac{\partial\phi^{\mathrm{el}}}{\partial\mathbf{A}^{\mathrm{el}}}\right) \tag{65}$$

governing the strictly reversible deformations. A simple reduction of Eq. (65) as stated in the undamaged case [Eq. (56)] is here not possible because $\phi^{\mathrm{el}}(\mathbf{A}^{\mathrm{el}}, \mathbf{A}^{\mathrm{da}})$ now involves anisotropic behavior due to the anisotropic evolution of damage. This fact will be discussed below when the elastic constitutive law will be formulated (see Section 4.2). In addition, according to the assumption that the changes in the internal structure of the matrix material and the evolution of damage are decomposed the Clausius–Duhem inequality can be separated into two parts

$$\left(\mathbf{R}\ \mathbf{T}\ \mathbf{R}^{-1}\right)\cdot\dot{\bar{\mathbf{H}}}^{\mathrm{pl}} - \rho_o\,\dot{\phi}^{\mathrm{pl}} \geqslant 0 \tag{66}$$

and

$$\tilde{\mathbf{T}}\cdot\dot{\mathbf{H}}^{\mathrm{da}} - \rho_o\,\frac{\partial\phi^{\mathrm{el}}}{\partial\mathbf{A}^{\mathrm{da}}}\cdot\dot{\mathbf{A}}^{\mathrm{da}} - \rho_o\,\dot{\phi}^{\mathrm{da}} \geqslant 0. \tag{67}$$

Please note that since the plastic potential function ϕ^{pl} with respect to the damaged configuration will not explicitly be formulated the positive plastic work dissipation requirement (66) will not be used in the present framework and, therefore, the plastic strain rate $\dot{\bar{\mathbf{H}}}^{\mathrm{pl}}$, which is based on the plastic potential function $\bar{\phi}^{\mathrm{pl}}$ with respect to the undamaged configuration, has only to enforce the condition (58). It may be assumed that ϕ^{pl} could be chosen in such a way that the dissipation inequality (66) will always be satisfied. The second dissipation positiveness requirement (67), on the other hand, will be used since the damage elastic and the damage potential function, ϕ^{el} and ϕ^{da}, will be considered. Eq. (67) may also be used to restrict the possibilities in formulating ϕ^{el} and, especially, may lead to restrictions for material parameters. Furthermore, from Eq. (67) it can be seen that the evolution equation for the damage part of the deformation will be expressed in terms of the damage strain rate $\dot{\mathbf{H}}^{\mathrm{da}}$ introduced kinematically by Eq. (41) and the damage condition will be expressed in terms of its work-conjugate stress tensor

$$\tilde{\mathbf{T}} = \mathbf{Q}^{\mathrm{el}}\,\mathbf{T}\,\mathbf{Q}^{\mathrm{el}-1}. \tag{68}$$

4. Constitutive equations

4.1. Effective undamaged configurations

The effective undamaged configurations are used to formulate the constitutive equations which adequately describe the elastic–plastic deformation behavior of the undamaged matrix material.

In particular, following, for example, Brünig (1999) the finite isotropic effective elastic part of the undamaged matrix material behavior is assumed to be governed by the effective Helmholtz free energy function

$$\rho_o\,\bar{\phi}^{\mathrm{el}}\left(\bar{\mathbf{A}}^{\mathrm{el}}\right) = G\ \bar{\mathbf{A}}^{\mathrm{el}}\cdot\bar{\mathbf{A}}^{\mathrm{el}} + \frac{1}{2}\left(K - \frac{2}{3}G\right)\left(\mathrm{tr}\bar{\mathbf{A}}^{\mathrm{el}}\right)^2 \tag{69}$$

where G and K represent the shear and bulk modulus of the matrix material, respectively. Taking into account the hyperelastic constitutive relationship (56) the effective stress tensor is expressed in the form

$$\bar{\mathbf{T}} = 2G\ \bar{\mathbf{A}}^{\mathrm{el}} + \left(K - \frac{2}{3}G\right)\mathrm{tr}\bar{\mathbf{A}}^{\mathrm{el}}\mathbf{1}. \tag{70}$$

If any effect of plastic straining on the finite effective elastic material behavior is neglected, the associated tensor of effective elastic moduli may be determined from

$$\mathbb{C} = \rho_o \frac{\partial^2 \bar{\phi}^{\mathrm{el}}}{\partial \bar{\mathbf{A}}^{\mathrm{el}} \otimes \partial \bar{\mathbf{A}}^{\mathrm{el}}} = 2G\ \mathbb{I} + \left(K - \frac{2}{3}G\right)\mathbf{1} \otimes \mathbf{1} \tag{71}$$

with the fourth order identity tensor

$$\mathbb{I} = \delta^i_k\, \delta^l_j\, \mathbf{g}_i \otimes \mathbf{g}^j \otimes \mathbf{g}_l \otimes \mathbf{g}^k. \tag{72}$$

Moreover, the yield condition is expressed in the form

$$f^{\mathrm{pl}}\left(\bar{\mathbf{T}}, c\right) = 0 \tag{73}$$

where c denotes the strength coefficient of the matrix material. Experimental studies on the effect of superimposed hydrostatic stress on the deformation behavior of metals carried out by Spitzig et al. (1975, 1976) have shown that the flow stress depends approximately linearly on hydrostatic stress state. Numerical studies presented by Brünig (1999) have elucidated that even small additional hydrostatic stress terms may remarkably effect the onset of localization as well as the associated deformation modes, and that they can lead to a notable decrease in ductility. Hence, plastic yielding of the matrix material is assumed to be adequately described by the yield condition

$$f^{\mathrm{pl}}\left(\bar{I}_1, \bar{J}_2, c\right) = \sqrt{\bar{J}_2} - c\left(1 - \frac{a}{c}\bar{I}_1\right) = 0, \tag{74}$$

where $\bar{I}_1 = \mathrm{tr}\bar{\mathbf{T}}$ and $\bar{J}_2 = \frac{1}{2}\mathrm{dev}\bar{\mathbf{T}}\cdot\mathrm{dev}\bar{\mathbf{T}}$ are invariants of the effective stress tensor $\bar{\mathbf{T}}$ and a represents the hydrostatic stress coefficient where a/c is a constant material parameter which has to be determined experimentally (Spitzig et al., 1975, 1976). In addition, the corresponding consistency condition is given by

$$\dot{f}^{\mathrm{pl}} = \left(\frac{1}{2\sqrt{\bar{J}_2}}\mathrm{dev}\bar{\mathbf{T}} + a\mathbf{1}\right)\cdot\dot{\bar{\mathbf{T}}} = \left(1 - \frac{a}{c}\bar{I}_1\right)\dot{c} = 0 \tag{75}$$

which will be used to determine the internal variables.

The effective plastic strain rate is assumed to be related to the current effective stress tensor through the flow rule which satisfies the positive work dissipation requirements (58). Thus, the plastic potential function $g^{\mathrm{pl}}(\bar{\mathbf{T}})$ is also formulated in terms of the effective stress tensor. In elastic-plastically deformed and damaged

metals irreversible volumetric strains are mainly caused by damage and, in comparison, volumetric plastic strains are negligible (see Spitzig et al., 1975). Thus, the plastic potential function

$$g^{\mathrm{pl}} = \sqrt{\bar{J}_2} \tag{76}$$

depends only on the second invariant of the effective stress deviator which leads to the isochoric effective plastic strain rate

$$\dot{\bar{\mathbf{H}}}^{\mathrm{pl}} = \dot{\lambda}\frac{\partial g^{\mathrm{pl}}}{\partial \bar{\mathbf{T}}} = \dot{\lambda}\frac{1}{2\sqrt{\bar{J}_2}}\mathrm{dev}\bar{\mathbf{T}} \tag{77}$$

where $\dot{\lambda}$ is a non-negative scalar-valued factor.

In addition, the normalized deviatoric tensor

$$\bar{\mathbf{N}} = \frac{1}{\sqrt{2\,\bar{J}_2}}\mathrm{dev}\bar{\mathbf{T}} \tag{78}$$

is introduced which leads to the definition of the equivalent plastic strain rate

$$\dot{\gamma} = \bar{\mathbf{N}}\cdot\dot{\bar{\mathbf{H}}}^{\mathrm{pl}} = \frac{1}{\sqrt{2}}\dot{\lambda} \tag{79}$$

which will be used to express the plastic strain rate tensor (77) in the form

$$\dot{\bar{\mathbf{H}}}^{\mathrm{pl}} = \dot{\gamma}\,\bar{\mathbf{N}}. \tag{80}$$

4.2. Anisotropically damaged configurations

The anisotropically damaged configurations are used to formulate the constitutive equations which adequately describe the deformation behavior of the damaged aggregate. In response of external loading the existence of microdefects results in an increase of the stress level in the remaining effective material and, on the other hand, in a decrease of the stored energy in the damaged material when compared to the response of the virgin undamaged material. To be able to describe these phenomena within the constitutive setting of a phenomenological elastic–plastic–damage framework the damaged elastic strain energy ϕ^{el}, which characterizes the elastic behavior of the damaged aggregate, is chosen to be an isotropic scalar function of the set of its arguments $\mathbf{A}^{\mathrm{el}}$ and $\mathbf{A}^{\mathrm{da}}$. For example, the most general form of the free energy function ϕ^{el} can be expressed by the combination of the 10 basic invariants of the two symmetric tensors $\mathbf{A}^{\mathrm{el}}$ and $\mathbf{A}^{\mathrm{da}}$ (see e.g. Lubarda and Krajcinovic, 1995; Hayakawa et al., 1998). In the initial undamaged state the ductile material is assumed to be isotropic and linear elastic and the elastic strain energy ϕ^{el} decreases with increasing damage. Thus, the function ϕ^{el} is taken to be quadratic in $\mathbf{A}^{\mathrm{el}}$ and linear in $\mathbf{A}^{\mathrm{da}}$ and the appropriate form of the damaged strain energy is then given by

$$\rho_o \phi^{\mathrm{el}}\left(\mathbf{A}^{\mathrm{el}}, \mathbf{A}^{\mathrm{da}}\right) = G\ \mathbf{A}^{\mathrm{el}}\cdot\mathbf{A}^{\mathrm{el}} + \frac{1}{2}\left(K - \frac{2}{3}G\right)\left(\mathrm{tr}\mathbf{A}^{\mathrm{el}}\right)^2 + \eta_1\,\mathrm{tr}\mathbf{A}^{\mathrm{da}}\left(\mathrm{tr}\mathbf{A}^{\mathrm{el}}\right)^2 + \eta_2\ \mathrm{tr}\mathbf{A}^{\mathrm{da}}\mathbf{A}^{\mathrm{el}}\cdot\mathbf{A}^{\mathrm{el}} + \eta_3\ \mathrm{tr}\mathbf{A}^{\mathrm{el}}\mathbf{A}^{\mathrm{da}}\cdot\mathbf{A}^{\mathrm{el}} + \eta_4\ \mathbf{A}^{\mathrm{el}}\cdot\left(\mathbf{A}^{\mathrm{el}}\mathbf{A}^{\mathrm{da}}\right) \tag{81}$$

where G and K are again the shear and bulk modulus of the undamaged matrix material and $\eta_1 \ldots \eta_4$ are material constants which describe the deterioration of the elastic properties by the occurrence of damage. The derivative

$$\rho_o \frac{\partial \phi^{\mathrm{el}}}{\partial \mathbf{A}^{\mathrm{el}}} = 2\left(G + \eta_2\,\mathrm{tr}\mathbf{A}^{\mathrm{da}}\right)\mathbf{A}^{\mathrm{el}} + \left[\left(K - \frac{2}{3}G + 2\eta_1\,\mathrm{tr}\mathbf{A}^{\mathrm{da}}\right)\mathrm{tr}\mathbf{A}^{\mathrm{el}} + \eta_3\left(\mathbf{A}^{\mathrm{da}}\cdot\mathbf{A}^{\mathrm{el}}\right)\right]\mathbf{1} + \eta_3\,\mathrm{tr}\mathbf{A}^{\mathrm{el}}\mathbf{A}^{\mathrm{da}} + \eta_4\left(\mathbf{A}^{\mathrm{el}}\mathbf{A}^{\mathrm{da}} + \mathbf{A}^{\mathrm{da}}\mathbf{A}^{\mathrm{el}}\right) \tag{82}$$

which is linear in $\mathbf{A}^{\mathrm{el}}$ and $\mathbf{A}^{\mathrm{da}}$, is used to determine the Kirchhoff stress tensor (65) of the damaged material. If $\mathbf{A}^{\mathrm{el}}$ is expressed in a series function in terms of $\mathbf{Q}^{\mathrm{el}}$, the derivative $\frac{\partial \mathbf{A}^{\mathrm{el}}}{\partial \mathbf{Q}^{\mathrm{el}}}$ will generally lead to a nonlinear expression in $\mathbf{Q}^{\mathrm{el}}$ and, thus, Eq. (65) yields a stress tensor which nonlinearly depends on $\mathbf{A}^{\mathrm{el}}$. As long as the material sample remains undamaged, the respective stress tensors $\mathbf{T}$ [Eq. (65)] and $\bar{\mathbf{T}}$ [Eq. (56)] should coincide and it is further assumed that $\mathbf{T}$ remains a linear function in $\mathbf{A}^{\mathrm{el}}$ when damage increases. Therefore, Eq. (65) is approximated by the constitutive relation

$$\mathbf{T} = \rho_o \frac{\partial \phi^{\mathrm{el}}}{\partial \mathbf{A}^{\mathrm{el}}} \tag{83}$$

and with Eq. (63) one gets

$$\mathbf{T}\cdot\dot{\mathbf{H}}^{\mathrm{el}} = \mathbf{T}\cdot\dot{\mathbf{A}}^{\mathrm{el}}. \tag{84}$$

Furthermore, the differential of Eq. (83) is given by

$$\mathrm{d}\mathbf{T} = \frac{\partial \mathbf{T}}{\partial \mathbf{A}^{\mathrm{el}}}\mathrm{d}\mathbf{A}^{\mathrm{el}} + \frac{\partial \mathbf{T}}{\partial \mathbf{A}^{\mathrm{da}}}\mathrm{d}\mathbf{A}^{\mathrm{da}} \tag{85}$$

where the partial derivatives can be written in the form

$$\mathbb{C}^{\mathrm{el}} = \frac{\partial \mathbf{T}}{\partial \mathbf{A}^{\mathrm{el}}} = 2\left(G + \eta_2\,\mathrm{tr}\mathbf{A}^{\mathrm{da}}\right)\mathbb{I} + \left(K - \frac{2}{3}G + 2\eta_1\,\mathrm{tr}\mathbf{A}^{\mathrm{da}}\right)\mathbf{1}\otimes\mathbf{1} + \eta_3\left(\mathbf{A}^{\mathrm{da}}\otimes\mathbf{1} + \mathbf{1}\otimes\mathbf{A}^{\mathrm{da}}\right) + \eta_4\ \mathbb{A}^{\mathrm{da}} \tag{86}$$

with

$$\mathbb{A}^{\mathrm{da}} = \left[\left(A^{\mathrm{da}}\right)^i_k \delta^l_j + \delta^i_k \left(A^{\mathrm{da}}\right)^l_j\right]\mathbf{g}_i \otimes \mathbf{g}^j \otimes \mathbf{g}_l \otimes \mathbf{g}^k \tag{87}$$

and

$$\mathbb{C}^{\mathrm{da}} = \frac{\partial \mathbf{T}}{\partial \mathbf{A}^{\mathrm{da}}} = 2\eta_1 \ \mathrm{tr}\mathbf{A}^{\mathrm{el}}\mathbf{1}\otimes\mathbf{1} + 2\eta_2\,\mathbf{A}^{\mathrm{el}}\otimes\mathbf{1} + \eta_3\,\mathbf{1}\otimes\mathbf{A}^{\mathrm{el}} + \eta_3 \ \mathrm{tr}\mathbf{A}^{\mathrm{el}}\mathbb{I} + \eta_4 \ \mathbb{A}^{\mathrm{el}} \tag{88}$$

with

$$\mathbb{A}^{\mathrm{el}} = \left[\left(A^{\mathrm{el}}\right)^i_k\delta^l_j + \delta^i_k\left(A^{\mathrm{el}}\right)^l_j\right]\mathbf{g}_i\otimes\mathbf{g}^j\otimes\mathbf{g}_l\otimes\mathbf{g}^k. \tag{89}$$

It should be noted that symmetry of $\mathbb{C}^{\mathrm{da}}$ holds as long as $2\eta_2 = \eta_3$. Eq. (86) clearly shows that the current elastic material properties are not constant and the influence of damage on the elastic behavior occurs as additional terms to the effective elastic constants, G and K. In particular, the first and second additional material constants, η_1 and η_2, are related to the isotropic character of damage whereas the third and fourth coefficient, η_3 and η_4, are due to anisotropic evolution of damage. Laboratory investigations on many ductile metals subjected to tensile stresses indicate that principal elastic moduli and the Poisson's ratios decrease as microdefects grow. These experimental observations place the physical bounds on the values of the additional constitutive parameters $\eta_1 \ldots \eta_4$ that they have to be taken to be negative. It should be noted that the decrease in the Poisson's ratio can not be described by standard isotropic as well as a large number of anisotropic damage models (see Ju, 1990) whereas the proposed damage approach is even able to simulate this experimentally observed effect.

Moreover, constitutive equations for damage evolution are required in the proposed theory of continuum damage mechanics. To determine the onset and the continuation of damage the concept of the damage surface is employed in analogy to the yield surface concept of the plasticity theory. However, unlike the yield condition (73) the form of the damage criterion is not well established. For example, Cordebois (1983) among many others employed a damage dissipation potential function formulated in terms of the so-called damage strain energy release rate. In order to overcome certain anomalies associated with the definition of the damage strain energy release rate tensor, discussed by Chow and Wang (1987), they instead formulated a damage dissipation potential in terms of their effective stress tensor. Similarly, the damage condition

$$f^{\mathrm{da}}\left(\tilde{\mathbf{T}}, \sigma\right) = 0 \tag{90}$$

is here expressed in terms of the stress tensor $\tilde{\mathbf{T}}$ (68), which is work-conjugate to the chosen damage strain rate tensor (41) [see Eq. (67)] and is formulated with respect to the elastically unloaded damaged configuration $\overset{*}{\mathcal{B}}$ (see Fig. 1), and σ denotes the damage threshold. In addition, the damage consistency condition

$$\dot{f}^{\mathrm{da}} = 0 \tag{91}$$

ensures that the current stress state satisfies the current damage condition during further loading histories and will be employed to determine the internal variables.

Furthermore, to be able to compute damage strain rates, the damage potential function $g^{\mathrm{da}}(\tilde{\mathbf{T}})$ is also formulated in terms of the stress tensor $\tilde{\mathbf{T}}$ providing a realistic physical representation of material degradation. This leads to the damage rule

$$\dot{\mathbf{H}}^{\mathrm{da}} = \dot{\mu}\,\frac{\mathrm{d}g^{\mathrm{da}}}{\mathrm{d}\tilde{\mathbf{T}}} \tag{92}$$

where $\dot{\mu}$ is a non-negative scalar-valued factor. The damage rule has to enforce the dissipation inequality (67). This leads to restrictions for the material parameters $\eta_1 \ldots \eta_4$ appearing in Eq. (81).

5. Macroscopic damage evolution model

The definition of the damage strain rate tensor (92) requires a damage evolution law which should be determined from realistic macroscopic damage propagation conditions. Therefore, experimental, theoretical and numerical studies have been performed to understand principal evolution modes of microcracks. Nowadays, it is well known, for example, that the development of microstructural cavities in ductile materials are generally governed by large strains of the material itself. Voids in structural metals nucleate from larger inclusions soon after the onset of plastic yielding and grow due to plastic deformations of the surrounding matrix material which play an important role in failure initiation. In addition, void size, void spacing and void distribution may remarkably affect further growth of existing voids and their coalescence, see e.g. Orsini and Zikry (2001), Khraishi et al. (2001), Taylor et al. (2002) and Li et al. (2003).

Several authors presented numerical studies and experimental observations on nucleation, growth and coalescence of voids leading to final fracture of tensile bars. For example, micromechanical cell model studies have been used to focus on void nucleation and growth to final failure. McClintock (1968) and Rice and Tracey (1969) have shown that the rates of growth of long cylindrical and spherical microscopic voids are significantly elevated by the superposition of hydrostatic tensile stresses on a remotely uniform plastic deformation field. The volume changing contribution to void growth is found to remarkably overwhelm the shape changing part when the mean remote normal stress is large. The void enlargement is amplified over the macroscopic strain rate by a factor arising exponentially with the ratio of the mean normal stress to the yield stress. In addition, Mackenzie et al. (1977) have shown that the onset of ductile damage in high strength steels strongly depends on the stress triaxiality. Since these results suggest a rapidly decreasing fracture ductility with increasing hydrostatic tension, realistic damage criteria must contain a term depending on the first stress invariant, $I_1 = \mathrm{tr}\mathbf{T} = \mathrm{tr}\tilde{\mathbf{T}}$, which may be seen as the dominating factor regulating the rate of creation and isotropic evolution of voids. Moreover, Tvergaard and Needleman (1984) analyzed round tensile bars to investigate the effect of mechanical properties on ductility. They first predicted void

formation and nearly isotropic void growth in plastically deformed regions and afterwards, after a critical void volume fraction has been passed, the onset of gross shear deformation with an associated coalescence of voids is observed thus indicating anisotropic damage behavior and, finally, leading to a central microcrack. These numerical results have been shown to be in good agreement with experimental observations reported by Bluhm and Morrissey (1965). In addition, Le Roy et al. (1981) discussed that nucleation and growth of voids were not separable and sequential processes. Voids nucleate continuously during straining and new voids are appearing while older ones are growing. As a result, nucleation and growth should be considered at the same time to be able to realistically describe the variation of porosity with increasing strains. They also have shown that in ductile materials a high deformation value is required to nucleate a significant number of voids and that void nucleation and growth mainly depend on the hydrostatic stress state.

Hence, provided that the initial void distribution is not too anisotropic, isotropic material behavior is taken into account at the early deformation stage and the damage of the material is assumed to be adequately described by the void volume fraction

$$f = \frac{\mathrm{d}v - \mathrm{d}\bar{v}}{\mathrm{d}v} \tag{93}$$

where $\mathrm{d}v$ denotes the differential volume of the current damaged configuration $\mathcal{B}$ and $\mathrm{d}\bar{v}$ represents the differential volume of the current undamaged configuration $\mathcal{E}$. Eq. (93) is expected to give a reasonable approximation up to a critical porosity f_c indicating the onset of void coalescence which then leads to highly anisotropic damage processes. Of course, this measure of damage, f, averages many variables, namely the number of voids, their sizes and shapes, the degree of adhesion between the voids, local variations of void density, local stress concentration effects and so forth, but it is assumed to be an adequate phenomenological parameter (see e.g. Tvergaard, 1990).

Following Brünig (2001) in the isotropic case the trace of the logarithmic damage strain tensor is given by

$$\mathrm{tr}\mathbf{A}^{\mathrm{da}} = \ln\frac{\mathrm{d}v}{\mathrm{d}\bar{v}} = \ln(1-f)^{-1} \tag{94}$$

and, consequently, the damage strain tensor (37) can be written in the form

$$\mathbf{A}^{\mathrm{da}} = \frac{1}{3}\ln(1-f)^{-1}\mathbf{1}. \tag{95}$$

The corresponding spheric part of the damage tensor is then expressed as

$$\overset{*}{\mathbf{R}} = (1-f)^{-2/3}\mathbf{1} \tag{96}$$

and making use of Eq. (41) one arrives at the damage strain rate tensor

$$\dot{\mathbf{H}}^{\mathrm{da}} = \frac{1}{3}(1-f)^{-1}\dot{f}\ \mathbf{1} \tag{97}$$

which describes the increase in isotropic growth of voids. Furthermore, based on experimental and numerical micromechanical observations discussed above the current isotropic damage behavior is assumed to be governed by the damage condition

$$f^{\mathrm{da}} = I_1 - \sigma = 0 \tag{98}$$

where σ represents the material toughness to void growth. Then the damage consistency condition (91) leads to

$$\dot{\sigma} = \dot{I}_1 = \mathrm{tr}\dot{\mathbf{T}} \tag{99}$$

and with the constitutive law (83) one arrives at

$$\dot{\sigma} = 3\tilde{K}\,\mathrm{tr}\dot{\mathbf{A}}^{\mathrm{el}} + \frac{3\tilde{\eta}}{1-f}\mathrm{tr}\mathbf{A}^{\mathrm{el}}\dot{f} \tag{100}$$

where the abbreviations

$$\tilde{K} = K + \tilde{\eta}\ln(1-f)^{-1} \tag{101}$$

and

$$\tilde{\eta} = 2\eta_1 + \frac{2}{3}(\eta_2 + \eta_3) + \frac{2}{9}\eta_4 \tag{102}$$

have been used.

In addition, the damage potential function

$$g^{\mathrm{da}}\left(\tilde{\mathbf{T}}\right) = \alpha I_1 \tag{103}$$

leads to the isotropic damage rule

$$\dot{\mathbf{H}}^{\mathrm{da}} = \dot{\mu}\frac{\mathrm{d}g^{\mathrm{da}}}{\mathrm{d}\tilde{\mathbf{T}}} = \dot{\mu}\alpha\mathbf{1} \tag{104}$$

which in comparison with the kinematically motivated Eq. (97) shows the identities

$$\dot{\mu} = \dot{f} \tag{105}$$

and

$$\alpha = \frac{1}{3}(1-f)^{-1}. \tag{106}$$

Eq. (105) clearly shows that the rate of the damage internal variable $\dot{\mu}$ represents the void volume fraction rate $\dot{f}$. In the numerical analyses reported below this parameter will be determined by enforcing the consistency conditions (75) and (91), see Brünig (2003) for further details. Moreover, several authors have proposed values of the critical void volume fraction f_c, which characterizes the onset of coalescence of cavities, based on experimental observations or finite element analyses in periodically voided ductile metals. Namely, Brown and Embury (1973) suggest that two neighboring cavities coalesce when their length has grown to the order of magnitude of their spacing. This local failure occurs by the development of slip planes in the

plastified matrix material between the cavities or simply by necking of the ligament. Based on their experimental results they estimated a critical void volume fraction for coalescence of about $f_c = 0.15$. However, experiments reported by Cialone and Asaro (1980) and Moussy (1985) have shown that lower void volume fractions were measured in structural alloys near the fracture surface in the center of the neck of round tensile test specimens. Therefore, the critical porosity $f_c = 0.15$ seems to be unrealistically large for real engineering materials.

The problem of determining the critical porosity f_c through micromechanical finite element simulations based on uniform or periodical distribution of voids has also been widely discussed in literature. A large number of numerical calculations, however, yield critical void volume fractions which are quite too large and, thus, lead to an overestimation of the overall ductility. One reason for the discrepancy is the assumed large initial void volume fraction which is not realistic in each case. For example, in engineering alloys voids generally form during straining by the decohesion or fracture of inclusions and, therefore, their initial porosity is very small. Only powder metallurgy consolidated alloys show significant initial porosity.

Numerical cell model studies by Becker et al. (1988) and Koplik and Needleman (1988) have shown that the value of f_c appears to vary slowly with stress triaxiality and matrix strain hardening but to depend strongly on the initial void volume fraction. In addition, numerical calculations reported by Dhar et al. (1996) have shown for a wide variation of plastic strains and stress triaxiality that the critical value of damage remains almost the same. Consequently, they regarded their critical damage parameter as a material property for prediction of microcrack initiation in ductile metals. Thus, taking f_c to depend only on the initial void volume fraction f but not on matrix hardening or stress triaxiality may be seen as a reasonable approximation. Then, based on the results of Becker et al. (1988), the critical void volume fraction f_c is taken to depend linearly on the initial porosity $\overset{o}{f}$:

$$f_c = 0.0344 + 1.25\,\overset{o}{f} \tag{107}$$

(see Fig. 2). Note that for smaller initial void volume fractions the values of f_c predicted by Eq. (107) are significantly lower than the value $f_c = 0.15$ suggested by Brown and Embury (1973) and taken into account by Tvergaard and Needleman (1984) within their numerical analyses.

However, real materials normally do not contain periodic but often strongly inhomogeneous distributions of voids. Experiments have shown that initial voids tend to be gathered in clusters. Then, coalescence must be accelerated in such a part of the material because it must start in the void clusters much earlier than it would do in a homogeneously voided material. This has been clearly established by Becker (1987) in his numerical study of nonhomogeneously voided solids and also by Magnusen et al. (1988) who studied experimentally the contrasting behavior of tensile metal specimens containing random and regular arrays of voids to provide a physical basis for understanding void linking during ductile microvoid fracture. In addition, Dubensky and Koss (1987) performed experiments to examine the sensitivity of ductile microvoid fracture processes on the size and distribution of voids,

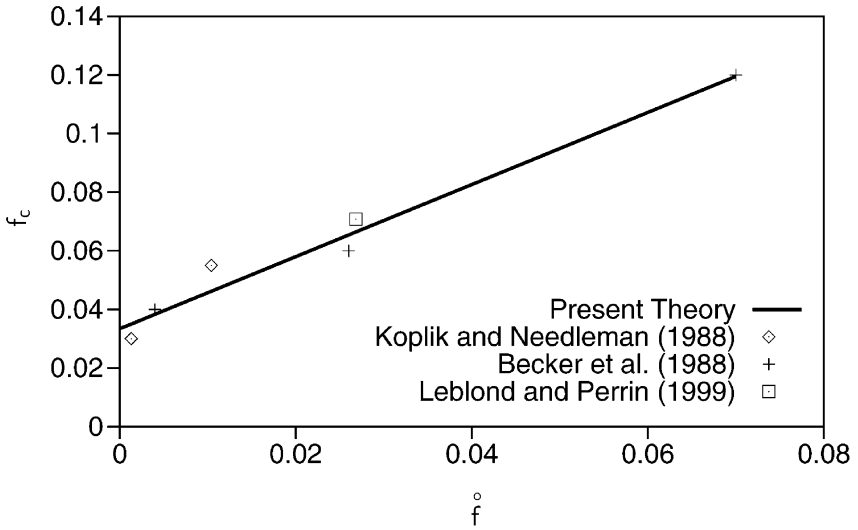

Fig. 2. Effect of initial porosity on critical void volume fraction.

and Melander and Stahlberg (1980) also analyzed the ductility of materials with different void distributions. Furthermore, Needleman and Kushner (1990) studied numerically the effect of various void distributions on the overall aggregate stress–strain response of initially porous inelastic solids. They found that the elastic material properties exhibit very low sensitivity to void distribution and, therefore, their degradation is assumed to be well described by the scalar parameter, f, in the isotropic case. Leblond and Perrin (1999) considered several distributions of initial void volume fraction with the same mean value $\overset{\circ}{f} = 0.0268$ and different standard deviations. Their self-consistent approach based on a model problem with hydrostatic load applied at infinity has shown a decrease of the critical void volume fraction f_c as the standard deviation of the initial void distribution increases. This means that porosity inhomogeneities favor coalescence. For example, the void distribution with the standard deviation of 0.006, which corresponds to actual measurement performed for engineering materials, leads to the critical void volume fraction $f_c = 0.0708$. This result is in good agreement with the critical porosity predicted by Eq. (107) and, therefore, the effect of random nature of experimentally observed void distributions on the critical void volume fraction is also included in the present phenomenological theory. Hence, when the current void volume fraction reaches a critical value $f = f_c$ (Eq. 107), the onset of coalescence of voids is predicted and the damage induced anisotropy caused by the changes in shape of the initially spherical microvoids is assumed to be important and has to be implemented into the present model.

Moreover, Jain et al. (1999) compared different criteria to predict the fracture limits of aluminum sheets for a variety of strain ratios. Their numerically predicted forming limit curves have shown that shear-type criteria lead to good agreement with experimental results for different strain paths. Microstructural observations of facture surfaces and through-thickness fracture characteristics confirm a shear-type

microvoid coalescence mechanism and subsequent fracture in aluminum sheets. Their qualitative observations show void growth and coalescence as well as the activation of shearing instabilities in the matrix material between the voids in direction of pure shear. Further experiments have shown that a combination of these two damage processes then leads to final fracture. In addition, Tvergaard and Needleman (1984) reported on events during tension of a round bar. They observed remarkable shear deformation with associated coalescence of voids leading to a microcrack which further grows in a zig-zag fashion. Based on careful examination of void growth and accumulation of damage during tensile loading, Le Roy et al. (1981) proposed sequential void nucleation and growth significantly depending on the hydrostatic stress whereas later coalescence of voids to oriented microcracks does not depend on hydrostatic stress. As a result, in the present model anisotropic damage behavior of ductile metals is assumed to be adequately described by the damage criterion

$$f^{\mathrm{da}}(I_1, J_2, \tilde{\sigma}) = I_1 + \tilde{\beta}\sqrt{J_2} - \tilde{\sigma} = 0 \tag{108}$$

which is a function of the stress invariants $I_1 = \mathrm{tr}\mathbf{T} = \mathrm{tr}\tilde{\mathbf{T}}$ and $J_2 = \frac{1}{2}\mathrm{dev}\mathbf{T}\cdot\mathrm{dev}\mathbf{T} = \frac{1}{2}\mathrm{dev}\tilde{\mathbf{T}}\cdot\mathrm{dev}\tilde{\mathbf{T}}$ to be able to take into account the hydrostatic and deviatoric stress effects caused by the shape and orientation of microdefects, and $\tilde{\sigma}$ denotes the material toughness to microcrack propagation. As long as uniaxial tension tests are used to determine the evolution equation for the equivalent aggregate stress measures σ and $\tilde{\sigma}$ appearing in the damage conditions (98) and (108) the relation $\tilde{\sigma} = \left(1 + \tilde{\beta}/\sqrt{3}\right)\sigma$ holds where σ denotes the uniaxial tension stress. In addition, in Eq. (108) the material property $\tilde{\beta}$ describes the influence of the deviatoric stress state on the damage condition.

Furthermore, to be able to compute damage strain rates, the damage potential function

$$g^{\mathrm{da}}\left(\tilde{\mathbf{T}}\right) = \alpha I_1 + \beta\sqrt{J_2} \tag{109}$$

is also formulated in terms of the stress tensor $\tilde{\mathbf{T}}$ providing a realistic physical representation of material degradation. In Eq. (109) α and β denote kinematically based damage parameters. Taking into account Eq. (92) this leads to the non-associated damage rule

$$\dot{\mathbf{H}}^{\mathrm{da}} = \dot{\mu}\alpha\mathbf{1} + \dot{\mu}\beta\frac{1}{2\sqrt{J_2}}\mathrm{dev}\tilde{\mathbf{T}}. \tag{110}$$

The first term in Eq. (110) represents the rate of inelastic volumetric deformations caused by the isotropic growth of microvoids whereas the second term is an explicit function of the deviatoric part of its work-conjugate stress tensor to be able to take into account the significant dependence of the evolution of size, shape and orientation of microdefects on the direction of the current stress state.

6. Numerical examples

6.1. Material characterization

Identification of continuum models consists in the quantitative evaluation of the chosen material coefficients characteristic of each material at each temperature considered. The determination of material parameters of the aggregate needs a measurement of damage which, however, is somewhat difficult due to the fact that damage does not affect very much any measurable quantity far from the rupture condition. Therefore, Spitzig et al. (1988) performed a large number of systematic experiments on iron compacts of different initial porosities to provide data that could be used to critically evaluate theoretical models of elastic–plastic behavior of porous ductile solids. They experimentally investigated mechanical properties of iron compacts as well as the effect of deformation on the evolution of void growth characteristics. These experimental data are used to determine the material parameters of the proposed anisotropic damage model.

In particular, taking into account the elastic constitutive Eq. (70) the elastic constants of the iron matrix material are chosen to be the shear modulus $G = 81\ 300$ MPa and the bulk modulus $K = 166\ 300$ MPa. In addition, the effective plastic parameters are estimated using experimental true stress–logarithmic plastic strain curves of fully dense tensile specimens. The nonlinear increase of the current strength coefficient c appearing in the yield condition (74) is numerically characterized by the power law

$$c = c_0\left(\frac{H_0\gamma}{n\ c_0} + 1\right)^n \tag{111}$$

to give the best fit to the experimental values. As can be seen from Fig. 3 the numerical simulation based on the initial yield strength $c_0 = 57.74$ MPa, the initial hardening parameter $H_0 = 5500$ MPa, and the hardening exponent $n = 0.296$ leads to good agreement with the experimental curve. In addition, based on the experiments reported by Spitzig and Richmond (1984) on the effect of superimposed pressure on the flow characteristics of metals the specific hydrostatic stress coefficient in Eq. (74) is chosen to be $a/c = 23\ \text{TPa}^{-1}$.

Furthermore, progressive damage often results in strain softening of the aggregate and the corresponding stress–strain curve exhibits a negative slope. This softening behavior leads to a loss in positive definiteness of the material tangent operator. Numerical analyses presented by Tvergaard and Needleman (1984), for example, suggested that during the increasing damage process the aggregate stress falls slowly until the void volume fraction reaches the critical value $f = f_c$ and, then, the aggregate stress drops abruptly with a remarkable loss of stress carrying capacity. Motivated by these results the equivalent aggregate stress–equivalent damage strain curve is approximated by a bilinear curve where the respective slopes $H^{\text{da}} = \frac{\mathrm{d}\sigma}{\mathrm{d}f}$ are chosen to be

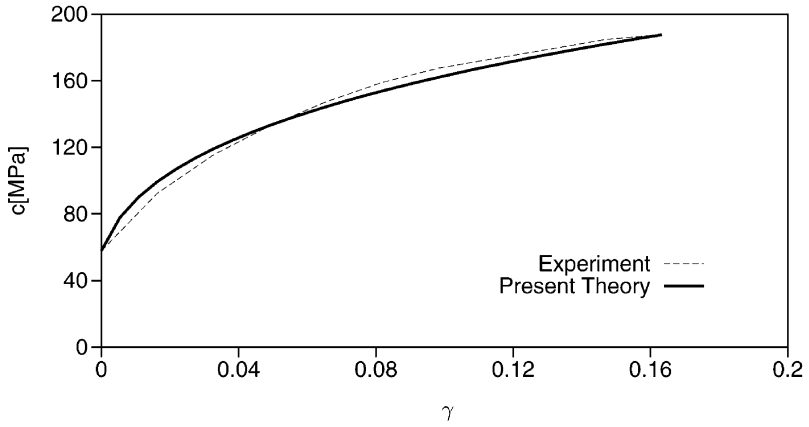

Fig. 3. Equivalent matrix stress–equivalent plastic strain curve.

$$H_1^{\mathrm{da}} = -50 \ \text{MPa} \ \text{ for } \ f < f_c \tag{112}$$

and

$$H_2^{\mathrm{da}} = -4000 \ \text{MPa} \ \text{ for } \ f \geqslant f_c, \tag{113}$$

where the critical void volume fraction, f_c, is given by Eq. (107).

Moreover, Spitzig et al. (1988) measured the elastic moduli of iron compacts with different porosities. These experimental results are used to determine the material parameters $\eta_1 \ldots \eta_4$ in Eq. (86) which describe the deteriorating influence of increasing damage on the elastic properties of the aggregate. For example, in the isotropic case Eq. (86) leads to the damaged elastic parameters: the damaged Young's modulus

$$E_d = \left[G + \left(\eta_2 + \frac{1}{3}\eta_4\right)\overset{*}{f}\right] \frac{3K + 2\left(3\eta_1 + \eta_2 + \eta_3 + \frac{1}{3}\eta_4\right)\overset{*}{f}}{K + \frac{1}{3}G + \left(2\eta_1 + \eta_2 + \frac{2}{3}\eta_3 + \frac{1}{3}\eta_4\right)\overset{*}{f}}, \tag{114}$$

the damaged shear modulus

$$G_d = G + \left(\eta_2 + \frac{1}{3}\eta_4\right)\overset{*}{f}, \tag{115}$$

the damaged bulk modulus

$$K_d = K + 2\left(\eta_1 + \frac{1}{3}\eta_2 + \frac{1}{3}\eta_3 + \frac{1}{9}\eta_4\right)\overset{*}{f}, \tag{116}$$

and the damaged Poisson's ratio

$$\nu_d = \frac{K - \frac{2}{3}G + 2\left(\eta_1 + \frac{1}{3}\eta_3\right)\overset{*}{f}}{2\left(K + \frac{1}{3}G\right) + 2\left(2\eta_1 + \eta_2 + \frac{2}{3}\eta_3 + \frac{1}{3}\eta_4\right)\overset{*}{f}}, \tag{117}$$

where the abbreviation

$$\overset{*}{f} = \ln(1-f)^{-1} \tag{118}$$

has been used. The four material constants $\eta_1 \ldots \eta_4$ are estimated by the fitting four experimental elastic moduli-porosity curves given by Spitzig et al. (1988). The respective parameters are chosen to be:

$$\eta_1 = -117\ 500\ \text{MPa}; \quad \eta_2 = -95\ 000\ \text{MPa};$$
$$\eta_3 = -190\ 000\ \text{MPa}; \quad \eta_4 = -255\ 000\ \text{MPa}.$$

Figs. 4–7 show the comparison for the Young's modulus, E_d, the shear modulus, G_d, the bulk modulus, K_d, and the Poisson's ratio, ν_d, versus the void volume fraction between experimental data and the predicted curves based on Eqs. (114)–(117) and the chosen parameters discussed above. In particular, remarkable decrease of E_d with increasing damage is observed in Fig. 4 and at $f=0.111$, E_d attains about 75% of its initial value. The available experimental data given by Spitzig et al. (1988) are accurately depicted by the curve given by Eq. (114). Similar results are shown in Figs. 5 and 6 where the numerically predicted shear and bulk moduli show very good agreement with the experiments. For example, at $f=0.111$ the shear modulus, G_d, and the bulk modulus, K_d, attain decreases of about 25% and 31% of their initial values, respectively. In addition, the present theory can precisely describe the experimentally observed decrease in the Poisson's ratio, see Fig. 7, which shows a final decrease of about 10%. Hence, the proposed anisotropic damage model is verified to properly depict the results of the relevant tests.

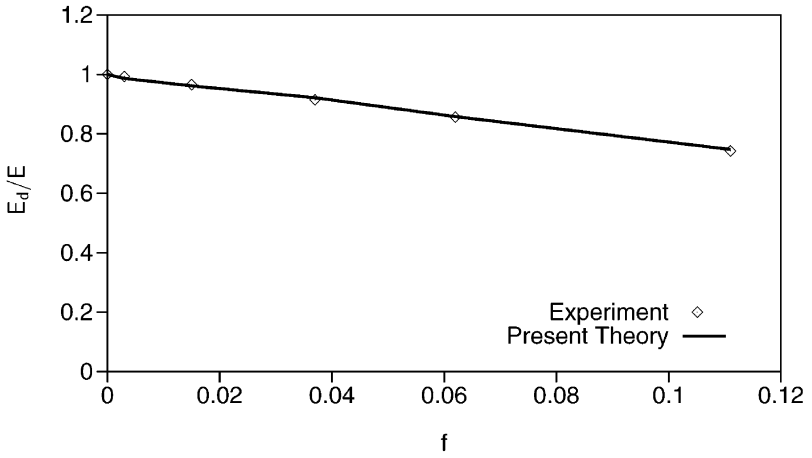

Fig. 4. Effect of porosity on the Young's modulus.

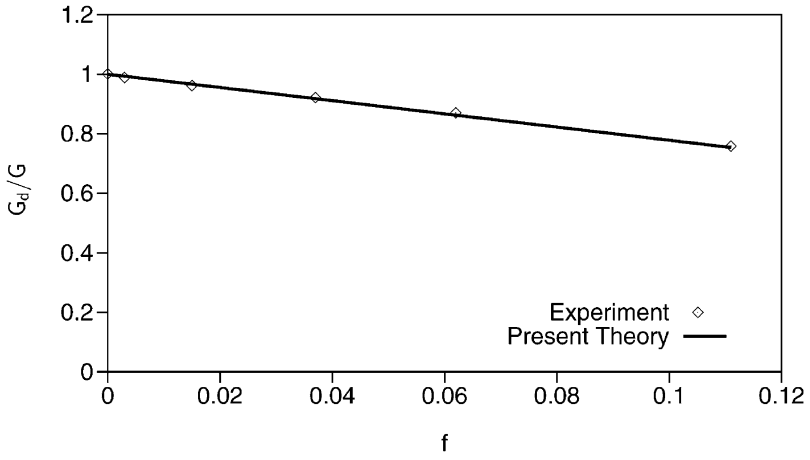

Fig. 5. Effect of porosity on the shear modulus.

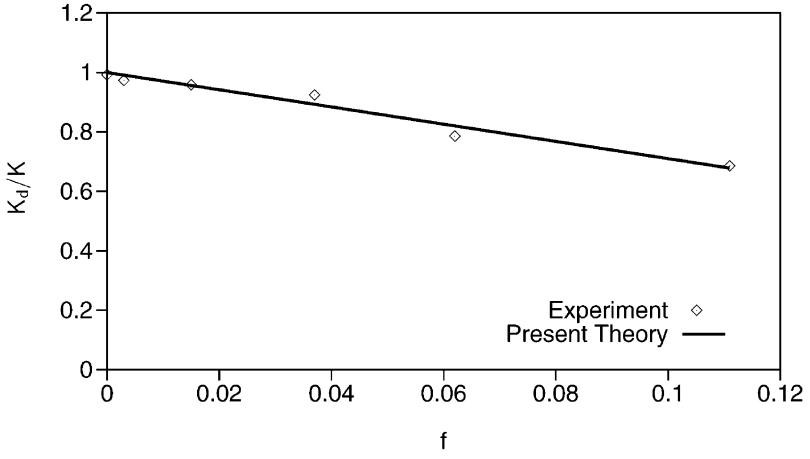

Fig. 6. Effect of porosity on the bulk modulus.

6.2. Tension tests under plane strain conditions

The present numerical analyses deal with the finite deformation behavior of uniaxially loaded geometrically perfect rectangular specimens with free ends. Finite element calculations take into account plane strain conditions and are based on the elastic–plastic–damage model with the constitutive parameters discussed above. It should be noted that in every step of the numerical calculation the requirement of damage dissipation positiveness (67) has to be checked. In the finite element analyses presented below Eq. (67) was always fulfilled what means that consistent damage parameters $\eta_1 \ldots \eta_4$ have been chosen.

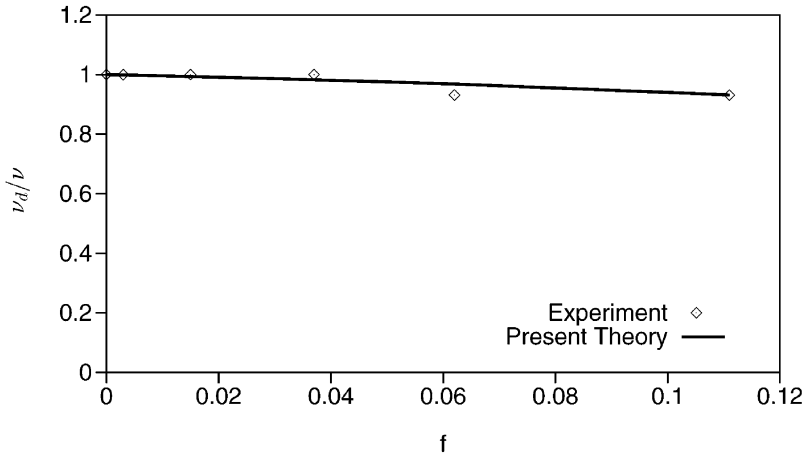

Fig. 7. Effect of porosity on the Poisson's ratio.

Fig. 8 shows the load–deflection curve which first shows a remarkable increase in load with increasing elastic–plastic deformations due to the work-hardening characteristics of the iron matrix material described by Eq. (111). The load has a maximum at the elongation $u/l = 0.157$ which is followed by a small sudden decrease in load of only about 1% corresponding to the onset of damage at the critical equivalent plastic strain $\gamma^{da} = 0.2$ and a slight subsequent load increase. This effect of beginning void growth on the overall load–deflection behavior has also been observed in the numerical analyses reported by Tvergaard and Needleman (1984). From $u/l = 0.188$ a small decrease in load with increasing deformation is observed.

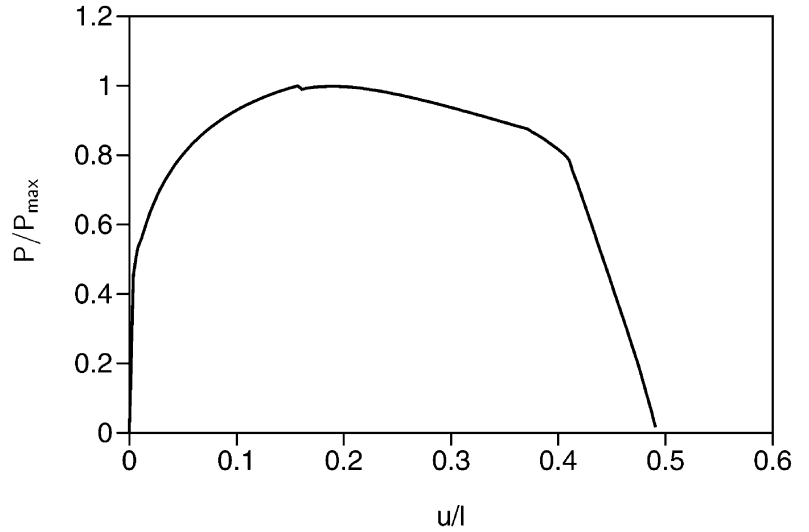

Fig. 8. Load–deflection curve.

Although the equivalent matrix stress–equivalent plastic strain curve (Fig. 3) still shows further work-hardening behavior this slow decrease is due to the decrease in the current specimen's area as well as in the decrease in the equivalent aggregate stress–equivalent damage strain curve given by Eq. (112) corresponding to the onset and growth of isotropic damage which results in decrease in aggregate stresses. Then, at the elongation $u/l = 0.412$ an abrupt drop in load is observed associated with a remarkable loss in load carrying capacity of the iron specimen. This fast decrease in load attributes to void coalescence and the subsequent formation and growth of microcracks thus leading to final fracture. This numerically predicted load–deflection behavior qualitatively agrees quite well with experiments and numerical calculations on ductile metal specimens reported by Tvergaard and Needleman (1984) and with experimental observations presented by Lemaitre and Dufailly (1987).

Fig. 9 illustrates the effect of the equivalent plastic strain on the current void volume fraction in a homogeneously deformed material element. In particular, after the onset of damage a nearly linear increase in porosity with increasing plastic deformation is observed. Afterwards, from $\gamma = 0.423$ the current porosity starts increasing much more rapidly with increasing plastic deformations. This effect is due to further void growth and simultaneous void coalescence which leads to the formation of microcracks. This numerically predicted behavior is qualitatively in good agreement with experimental results reported by Spitzig et al. (1988).

The development of the damage strain components A_{11}^{da} in the tensile loading direction and A_{22}^{da} perpendicular to the loading axis with increasing elongation of the tensile specimen is shown in Fig. 10. As long as damage remains isotropic ($f < f_c$) both damage strain components coincide and they show a nearly linear increase. Afterwards, from $f \geqslant f_c$, however, the damage strain in loading direction, A_{11}^{da}, shows a remarkable faster increase whereas the damage strain perpendicular to the loading axis, A_{22}^{da}, increases more slowly which implies considerable anisotropic evolution of

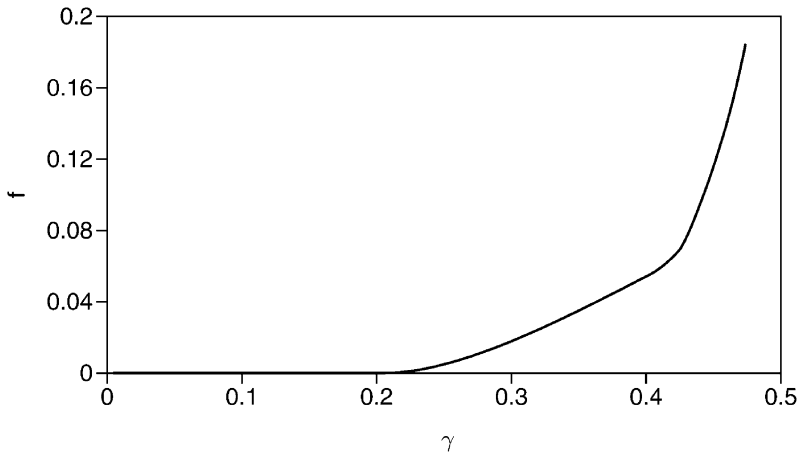

Fig. 9. Current void volume fraction vs. equivalent plastic strain.

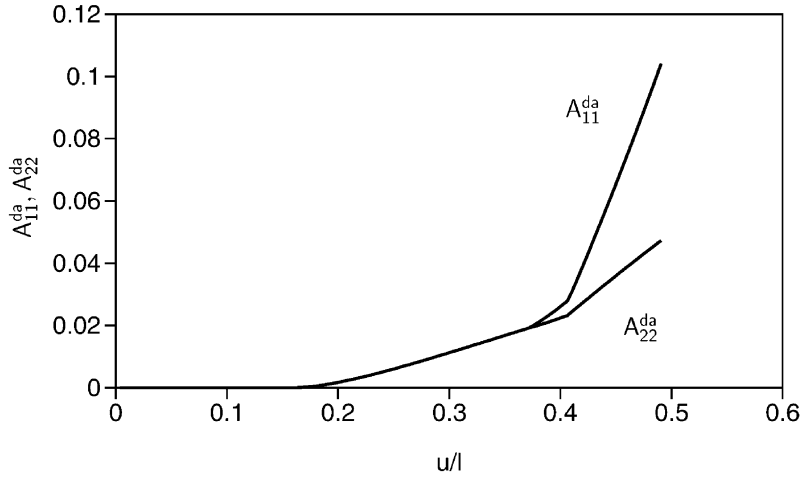

Fig. 10. Damage strain components vs. elongation.

the damage. At final elongation $u/l=0.491$, for example, the damage strain A_{22}^{da} remains only 45% of the final value of A_{11}^{da} caused by the anisotropic coalescence of voids and growth of microcracks.

7. Conclusions

A phenomenological anisotropic damage model for ductile metals undergoing progressive plastic-deformation-induced material deterioration has been discussed. A characteristic feature of the present continuum approach is the kinematic description of anisotropic damage which employs the consideration of damaged as well as fictitious undamaged configurations related via metric transformations which allow for the interpretation of damage tensors. The modular structure is accomplished by the kinematic decomposition of strain rates into elastic, plastic and damage parts. Respective Helmholtz free energy functions of the fictitious undamaged configuration and of the current damaged configuration are introduced separately which allow the formulation of elastic constitutive laws for both the matrix material and the damaged aggregate. Thus, the model does not need strain equivalence, stress equivalence or strain energy equivalence approaches often used in continuum damage theories to be able to connect matrix material and aggregate variables. Since plastic flow and damage are distinctly different irreversible processes in their nature plastic constitutive equations are formulated in an effective stress space whereas the evolution equation of the anisotropic damage strain rate tensor is given in the damaged aggregate stress space.

The applicability of the proposed continuum damage theory is demonstrated by the numerical simulation of the deformation behavior of ductile metals. The phenomenological model is ascertained to properly describe the results of the relevant

tests. For example, the present approach accurately depicts the deteriorating effect of increasing porosity on elastic moduli and realistically predicts the anisotropic damage behavior of tension specimens. It realistically follows the inception of plastic deformations through the initiation and isotropic growth of voids to void coalescence and the linking up of these voids in microcracks which corresponds to a sudden and remarkable decrease in load carrying capacity of tension specimens. This softening behavior corresponds to a loss in positive definiteness of the material tangent operator which leads in the numerical calculation of tensile specimens or more complex engineering structures to non uniqueness in the solution as well as to localization phenomena which will be discussed in a forthcoming paper. Hence, the present approach deals with the whole damage accumulation process till final fracture of structural integrity. This offers a complementary alternative to conventional fracture mechanics. In addition, the proposed large strain damage theory may be seen as a powerful basic framework to develop structural models capable for providing practical solutions of general problems in engineering.

References

Alves, M., Yu, J., Jones, N., 2000. On the elastic modulus degradation in continuum damage mechanics. Comp. Struct. 76, 703–712.

Alves, M., 2001. Measurement of ductile material damage. Mech. Struct. Mach. 29, 451–476.

Asaro, R., 1983. Micromechanics of crystals and polycrystals. Adv. Appl. Mech. 23, 1–115.

Baste, S., Audoin, B., 1991. On internal variables in anisotropic damage. Eur. J. Mech., A/Solids 10, 587–606.

Becker, R., 1987. The effect of porosity distribution on ductile failure. J. Mech. Phys. Solids 35, 577–599.

Becker, R., Needleman, A., Richmond, O., Tvergaard, V., 1988. Void growth and failure in notched bars. J. Mech. Phys. Solids 36, 317–351.

Betten, J., 1982. Net-stress analysis in creep mechanics. Ingenieur-Archiv. 52, 405–419.

Betten, J., 1983. Damage tensors in continuum mechanics. J. Méc. Théor. Appl. 2, 13–32.

Bluhm, J.I., Morrissey, R.J., 1965. Fracture in a tensile specimen. In: Proc. 1st Int. Conf. Fracture, Vol. 3, Sendai, 1739.

Brown, L.M., Embury, J.D., 1973. The initiation and growth of voids at second phase particles. In: Proc. 3rd Int. Conf. on Strength of Metals and Alloys, Inst. of Metals, London, pp. 164–169.

Brünig, M., 1999. Numerical simulation of the large elastic-plastic deformation behavior of hydrostatic stress-sensitive solids. Int. J. Plasticity 15, 1237–1264.

Brünig, M., 2001. A framework for large strain elastic-plastic damage mechanics based on metric transformations. Int. J. Eng. Science 39, 1033–1056.

Brünig, M., 2003. Numerical analysis of anisotropic ductile continuum damage. Comp. Meth. Appl. Mech. Engng. (submitted for publication).

Bruhns, O.T., Schiesse, P., 1996. A continuum model of elastic-plastic materials with anisotropic damage by oriented microvoids. Eur. J. Mech., A/Solids 15, 367–396.

Chaboche, J.L., 1984. Anisotropic creep damage in the framework of continuum damage mechanics. Nuclear Engng. Design 79, 309–319.

Chaboche, J.L., 1988a. Continuum damage mechanics: Part I—general concepts. J. Appl. Mech. 55, 59–64.

Chaboche, J.L., 1988b. Continuum damage mechanics: Part II—damage growth, crack initiation, and crack growth. J. Appl. Mech. 55, 65–72.

Chow, C.L., Wang, J., 1987. An anisotropic theory of continuum damage mechanics for ductile fracture. Eng. Frac. Mech. 27, 547–558.

Cialone, H., Asaro, R.J., 1980. Hydrogen assisted fracture of spherodized plain carbon steels. Met. Trans. 12A, 1373–1387.
Cordebois, J.P., 1983. Critères d'Instabilité Plastique et Endommagement Ductile en Grandes Deformation. Thèse de Doctorat, Univ. Paris VI, France.
Dhar, S., Sethuraman, R., Dixit, P.M., 1996. A continuum damage mechanics model for void growth and micro crack initiation. Eng. Fract. Mech. 53, 917–928.
Dubensky, E.M., Koss, D.A., 1987. Void/pore distributions and ductile fracture. Metal. Trans. A 18A, 1887–1895.
Grabacki, J., 1991. On some desciption of damage processes. Eur. J. Mech., A/Solids 10, 309–325.
Hayakawa, K., Murakami, S., Liu, Y., 1998. An irreversible thermodynamics theory for elastic-plastic-damage materials. Eur. J. Mech., A/Solids 17, 13–32.
Jain, M., Allin, J., Lloyd, D.J., 1999. Fracture limit prediction using ductile fracture criteria for forming of an automotive aluminum sheet. Int. J. Mech. Sci. 41, 1273–1288.
Ju, J.W., 1990. Isotropic and anisotropic damage variables in continuum damage mechanics. J. Eng. Mech. 116, 2764–2770.
Kachanov, L.M., 1958. On rupture time under condition of creep. Izvestia Akademi Nauk USSR, Otd. Techn. Nauk, Moskwa 8, 26–31.
Kachanov, M., 1980. Continuum model of medium with cracks. J. Eng. Mech. Div. 106, 1039–1051.
Khraishi, T.A., Khaleel, M.A., Zbib, H.M., 2001. A parametric-experimental study of void growth in superplastic deformation. Int. J. Plasticity 17, 297–315.
Koplik, J., Needleman, A., 1988. Void growth and coalescence in porous plastic solids. Int. J. Solids Structures 24, 835–853.
Krajcinovic, D., 1983. Constitutive equations for damaging materials. J. Appl. Mech. 50, 355–360.
Krajcinovic, D., 1989. Damage mechanics. Mech. Mater. 8, 117–197.
Krajcinovic, D., Fonseka, G.U., 1981a. The continuous damage theory of brittle materials. Part 1: general theory. J. Appl. Mech. 48, 809–815.
Krajcinovic, D., Fonseka, G.U., 1981b. The continuous damage theory of brittle materials. Part 2: uniaxial and plane response modes. J. Appl. Mech. 48, 816–824.
Leblond, J.-B., Perrin, G., 1999. A self-consistent approach to coalescence of cavities in inhomogeneously voided ductile solids. J. Mech. Phys. Solids 47, 1823–1841.
Lehmann, Th., 1989. Some thermodynamical considerations on inelastic deformations including damage processes. Acta Mech. 79, 1–24.
Lehmann, Th., 1991. Thermodynamical foundations of large inelastic deformations of solid bodies including damage. Int. J. Plasticity 7, 79–98.
Lemaitre, J., 1985a. A continuous damage mechanics model for ductile fracture. J. Eng. Mater. Tech. 107, 83–89.
Lemaitre, J., 1985b. Coupled elasto-plasticity and damage constitutive equations. Comp. Meth. Appl. Mech. Eng. 51, 31–49.
Lemaitre, J., 1986. Local approach of fracture. Eng. Frac. Mech. 25, 523–537.
Lemaitre, J., 1996. A Course on Damage Mechanics, second ed. Springer, Berlin.
Lemaitre, J., Dufailly, J., 1987. Damage measurements. Eng. Fract. Mech. 28, 643–661.
Le Roy, G., Embury, J.D., Edward, G., Ashby, M.F., 1981. A model of ductile fracture based on the nucleation and growth of voids. Acta Metall. 29, 1509–1522.
Li, Z., Wang, C., Chen, C., 2003. The evolution of voids in the plasticity strain hardening gradient materials. Int. J. Plasticity 19, 213–234.
Lu, T.J., Chow, C.L., 1990. On constitutive equations of inelastic solids with anisotropic damage. Theor. Appl. Fract. Mech. 14, 187–218.
Lubarda, V.A., Krajcinovic, D., 1993. Damage tensors and crack density distribution. Int. J. Solids Struct. 30, 2859.
Lubarda, V.A., Krajcinovic, D., 1995. Some fundamental issues in rate theory of damage-elastoplasticity. Int. J. Plasticity 11, 763–797.
Mackenzie, A.C., Hancock, J.W., Brown, D.K., 1977. On the influence of state of stress on ductile failure initiation in high strength steels. Eng. Fract. Mech. 9, 167–188.

Magnusen, P.E., Dubensky, E.M., Koss, D.A., 1988. The effect of void arrays on void linking during ductile fracture. Acta Metall. 36, 1503–1509.

McClintock, F.A., 1968. A criterion for ductile fracture by growth of holes. J. Appl. Mech. 35, 363–371.

Melander, A., Stahlberg, U., 1980. The effect of void size and distribution on ductile fracture. Int. J. Fracture 16, 431–440.

Moussy, F., 1985. Les differentes echelles du developpement de l'endommagement dans del aciers. Influence sur la localization de la deformation a l'echelle microscopique. In: Salencon, J. (Ed.), Proc. Int. Symp. on Plastic Instability—Considere Memorial, Presses Ponts et Chaussees, pp. 263–272.

Murakami, S., 1988. Mechanical modeling of material damage. J. Appl. Mech. 55, 280–286.

Murakami, S., Ohno, N., 1981. A continuum theory of creep and creep damage. In: Ponter, A.R.S., Hayhurst, D.R. (Eds.), Creep in Structures. Springer Verlag, Berlin, pp. 422–443.

Needleman, A., Kushner, A.S., 1990. An analysis of void distribution effects on plastic flow in porous solids. Eur. J. Mech., A/Solids 9, 193–206.

Orsini, V.C., Zikry, M.A., 2001. Void growth and interaction in crystalline materials. Int. J. Plasticity 17, 1393–1417.

Rabotnov, I.N., 1963. On the equations of state for creep. In: Progress in Appl. Mech.—The Prager Anniversary Volume. MacMillan, New York, pp. 307–315.

Rice, J.R., Tracey, D.M., 1969. On the ductile enlargement of voids in triaxial stress fields. J. Mech. Phys. Solids 17, 201–217.

Simo, J.C., Ju, J.W., 1987. Strain- and stress-based continuum damage models—I. Formulation. Int. J. Solids Structures 23, 821–840.

Spitzig, W.A., Richmond, O., 1984. The effect of pressure on the flow stress of metals. Acta Metall. 32, 457–463.

Spitzig, W.A., Smelser, R.E., Richmond, O., 1988. The evolution of damage and fracture in iron compacts with various initial porosities. Acta Metall. 36, 1201–1211.

Spitzig, W.A., Sober, R.J., Richmond, O., 1975. Pressure dependence of yielding and associated volume expansion in tempered martensite. Acta Metall. 23, 885–893.

Spitzig, W.A., Sober, R.J., Richmond, O., 1976. The effect of hydrostatic pressure on the deformation behavior of maraging and HY-80 steels and its implications for plasticity theory. Metall. Trans. 7A, 1703–1710.

Steinmann, P., Carol, I., 1998. A framework for geometrically nonlinear continuum damage mechanics. Int. J. Eng. Sci. 36, 1793–1814.

Taylor, M.B., Zbib, H.M., Khaleel, M.A., 2002. Damage and size effects during superplastic deformation. Int. J. Plasticity 18, 415–442.

Tvergaard, V., 1990. Material failure by void growth to coalescence. Adv. Appl. Mech. 27, 83–151.

Tvergaard, V., Needleman, A., 1984. Analysis of the cup-cone fracture in a round tensile bar. Acta Metall. 32, 157–169.

Voyiadjis, G.Z., Kattan, P.I., 1992. A plasticity-damage theory for large deformation of solids—I. Theoretical formulation. Int. J. Eng. Sci. 30, 1089–1108.

Voyiadjis, G.Z., Kattan, P.I., 1999. Advances in Damage Mechanics: Metals and Metal Matrix Composites. Elsevier, Amsterdam.

Voyiadjis, G.Z., Park, T., 1999. The kinematics of damage for finite-strain elasto-plastic solids. Int. J. Eng. Sci. 37, 803–830.